Sediment Melts at Sub-arc Depths: an Experimental Study

JÖRG HERMANN[1]* AND CARL J. SPANDLER[2]

[1]RESEARCH SCHOOL OF EARTH SCIENCES, THE AUSTRALIAN NATIONAL UNIVERSITY, CANBERRA, A.C.T. 0200, AUSTRALIA

[2]INSTITUTE OF GEOLOGICAL SCIENCES, UNIVERSITY OF BERN, CH-3012 SWITZERLAND

RECEIVED APRIL 30, 2007; ACCEPTED OCTOBER 16, 2007
ADVANCE ACCESS PUBLICATION DECEMBER 4, 2007

*The phase and melting relations in subducted pelites have been investigated experimentally at conditions relevant for slabs at sub-arc depths (*T = *600–1050°C,* P = *2·5–4·5 GPa). The fluid-present experiments produced a dominant paragenesis consisting of garnet–phengite–clinopyroxene–coesite–kyanite that coexists with a fluid phase at run conditions. Garnet contains detectable amounts of* Na_2O *(up to 0·5 wt%),* P_2O_5 *(up to 0·56 wt%), and* TiO_2 *(up to 0·9 wt%) in all experiments. Phengite is stable up to 1000°C at 4·5 GPa and is characterized by high* TiO_2 *contents of up to 2 wt%. The solidus has been determined at 700°C, 2·5 GPa and is situated between 700 and 750°C at 3·5 GPa. At 800°C, 4·5 GPa glass was present in the experiments, indicating that at such conditions a hydrous melt is stable. In contrast, at 700°C, 3·5 and 4·5 GPa, a solute-rich, non-quenchable aqueous fluid was present. This indicates that the solidus is steeply sloping in* P–T *space. Fluid-present (vapour undersaturated) partial melting of the pelites occurs according to a generalized reaction phengite + omphacite + coesite + fluid = melt + garnet. The* H_2O *content of the produced melt decreases with increasing temperature. The* K_2O *content of the melt is buffered by phengite and increases with increasing temperature from 2·5 to 10 wt%, whereas* Na_2O *decreases from 7 to 2·3 wt%. Hence, the melt compositions change from trondhjemitic to granitic with increasing temperature. The* K_2O/H_2O *increases strongly as a function of temperature and nature of the fluid phase. It is 0·0004–0·002 in the aqueous fluid, and then increases gradually from about 0·1 at 750–800°C to about 1 at 1000°C in the hydrous melt. This provides evidence that hydrous melts are needed for efficient extraction of K and other large ion lithophile elements from subducted sediments. Primitive subduction-related magmas typically have* K_2O/H_2O *of ~0·1–0·4, indicating that hydrous melts rather than aqueous fluids are responsible for large ion lithophile element transfer in subduction zones and that top-slab temperatures at sub-arc depths are likely to be 700–900°C.*

KEY WORDS: *experimental petrology; pelite; subduction; UHP metamorphism; fluid; LILE*

INTRODUCTION

Subducted sediments play a key role in the recycling of incompatible elements in subduction zones. The comparison of primitive arc lavas with mid-ocean ridge basalts (MORB) provides evidence that arc lavas are enriched in H_2O, large-ion lithophile elements (LILE) and, to a lesser extent, light rare earth elements (LREE) (Tatsumi & Eggins, 1995). The enrichment of these components is interpreted to be related to the addition of a 'slab component' to the locus of partial melting in the mantle wedge (Hawkesworth *et al.*, 1993). Detailed chemical analyses of oceanic crustal material have revealed that subducted sediments are the dominant host of LILE in the slab (Plank & Langmuir, 1998; Tenthorey & Hermann, 2004). The fundamental role of sediments in the recycling of LILE has also been demonstrated by the matching of trace element ratios of sediment input and arc output in several subduction zones (e.g. Plank & Langmuir, 1993; Peate *et al.*, 1997). Therefore, the systematic study of subducted sediments is crucial for understanding the LILE transfer. The pressure range where this transfer occurs is constrained by the depth (70–170 km) of the subducted slab below the volcanic arc (Tatsumi, 1986; Syracuse & Abers, 2006). Hence, it is important to study phase and melting relations

*Corresponding author. Telephone: ++61 2 6125 8842. E-mail: joerg.hermann@anu.edu.au

in subducted sediments that experienced pressures in the range of 2·5–5 GPa.

One approach to study such phase relations is through investigation of ultrahigh-pressure (UHP) metamorphic rocks (Hermann *et al.*, 2006). Subducted continental crust occasionally contains relics of coesite and diamond, providing evidence that these rocks were metamorphosed at 100–150 km depth (Chopin, 1984; Sobolev & Shatsky, 1990). Metapelites, metagranites and metacarbonates in such terrains can be used as natural laboratories to study phase and melting relations in subducted sediments (Philippot *et al.*, 1995; Stöckhert *et al.*, 2001; Hermann *et al.*, 2006). Bulk-rock and mineral trace element analyses of such rocks have shown that phengite plays a key role as a repository for LILE (Sorenson *et al.*, 1997; Spandler *et al.*, 2003). However, one major problem with the interpretation of such data is that deeply subducted rocks cool relatively slowly during exhumation and hence it is not clear whether the original chemical signature of phases is preserved. Moreover, in these rocks the record of the fluid phase is, at best, only fragmentarily preserved, and so little information on the composition and nature of the fluid phase present at UHP conditions can be obtained.

High-pressure experiments on sedimentary bulk compositions provide a second way of investigating element recycling in subduction zones. Experimental studies are important for understanding mineral relations in subducted sediments and for directly constraining the composition and nature of the fluid phase. Experimental studies have confirmed that phengite is the stable K-phase in subducted sediments at sub-arc depths (Domanik & Holloway, 1996; Schmidt, 1996; Ono, 1998; Hermann, 2002*b*; Auzanneau *et al.*, 2006). Consequently, an understanding of phengite melting relations is crucial for understanding the recycling of LILE. One of the problems with experimental studies is that piston cylinder techniques are used at pressures $\leq$3·5 GPa, whereas multi-anvil experiments are used at pressures $\geq$3·5 GPa (Schmidt *et al.*, 2004). This might introduce some systematic errors exactly in the critical pressure range where the subduction-zone fluids leave the slab.

There are contrasting views on the nature and composition of the fluid phase that transports the key elements from the slab to the mantle wedge. Geochemical studies of arc magmas have attempted to constrain the nature of the fluid phase on the basis of element ratios. Two end-members have been proposed corresponding to a sediment fluid component and a sediment melt component (Class *et al.*, 2000; Elliott, 2003). However, it must be stressed that the actual phase relations and buffering phases in the slab are often ignored. A second approach to constrain the nature and composition of the fluid phase involves detailed solubility studies of minerals in fluids and calculation of fluid compositions in equilibrium with the determined high-pressure phases (Manning, 1998, 2004). Such an approach has provided excellent results for major element concentrations in the aqueous fluid. To establish whether an aqueous fluid or a hydrous melt is leaving the subducted slab, it is necessary to combine expected top-slab temperatures with experimental studies on the solidus of sedimentary rocks (Nichols *et al.*, 1994; Hermann *et al.*, 2006). To date, this approach has been inconclusive because there exists a large variation in predicted top-slab temperatures according to different models, as well as discrepancies in the position of the wet solidus for typical subducted sediments. A further complication arises as a consequence of the potential presence of the second critical endpoint (Kessel *et al.*, 2005*b*). In the pelitic system the termination of the wet solidus at the second critical endpoint might be reached at pressure and temperature conditions relevant for subducted sediments at sub-arc depth, and hence transitional supercritical fluids could be the transporting agent (Manning, 2004; Kessel *et al.*, 2005*a*; Hermann *et al.*, 2006).

In this paper we present the results of an experimental study on the phase and melting relations in a pelite composition. We used piston cylinder experiments for the entire dataset covering a P–T range of 2·5–4·5 GPa and 600–1050°C, appropriate for sub-arc conditions. This eliminates any potential systematic errors involved in using two different experimental techniques. We systematically investigated the stability and melting behaviour of phengite to constrain the recycling of K_2O from subducted sediments. Fluid-present melting is explored and special emphasis is placed on constraining the position of the wet solidus. We show that the compositions of aqueous fluids and hydrous melts vary as a function of temperature, and we use this information to postulate that sediment melts provide the simplest way to explain the K_2O and H_2O systematics of primitive arc lavas. We also report how the common UHP phases garnet, omphacite and phengite change their composition as a function of pressure and temperature and how this information can be used as a guide to evaluate how well UHP rocks preserve original phase compositions.

EXPERIMENTAL METHODS

Starting material

A starting material has been synthesized with a major-element composition similar to average global subducting sediment (GLOSS; Plank & Langmuir, 1998) and the average upper continental crust (Fig. 1; Taylor & McLennan, 1985). The starting material was produced using a 'sol–gel' method to eliminate problems of sluggish reaction of refractory minerals during experiments. Most major elements and some trace elements (Spandler *et al.*, 2007*b*) were combined as nitrate solutions and mixed with tetraethyl orthosilicate [$Si(C_2H_5O)_4$] and slowly dried

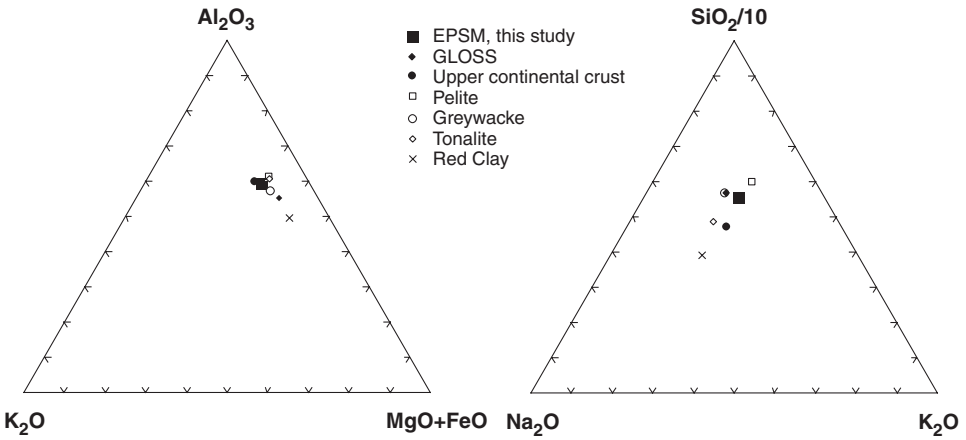

Fig. 1. Triangular projection of the experimental pelite starting material (EPSM) used in this study compared with global oceanic subducted sediment (GLOSS; Plank & Langmuir, 1998), and upper continental crust (Taylor & McLennan, 1985), as well as starting materials from other experimental studies [pelite from Schmidt *et al.* (2004); greywacke from Auzanneau *et al.* (2006); tonalite from Patiño Douce (2005); red clay from Johnson & Plank (1999)].

to a gel. From this basic gel, two starting materials were prepared that differ only in their H_2O content. For the anhydrous starting material, the gel was combined with appropriate amounts of Al_2O_3, TiO_2 and MnO powders, finely milled and then fused at 1500°C and quenched to glass. Multiple analyses of the glass for major elements (by energy-dispersive spectrometry; EDS) and trace elements (by laser ablation inductively coupled plasma mass spectrometry; LA-ICP-MS) indicate homogeneity within analytical precision. Iron was then added to the glass in the form of synthetic fayalite. The fayalite and glass mixture was ground for 30 min to form a fine powder. For the hydrous starting material, no Al_2O_3 was added prior to melting. Instead, $Al(OH)_3$, in a quantity sufficient to produce the same amount of Al_2O_3 as in the anhydrous starting material, was added together with fayalite at the end. This second starting material contains 6·8 wt% H_2O. Blending of the hydrous and anhydrous starting materials permitted us to obtain precise but variable H_2O contents in the experiments, which provide the basis for determination of melt H_2O contents using mass balance. The water content of high-pressure melts increases with decreasing temperature (Hermann, 2003). To maintain 15–25% of hydrous melt in the experiments, which facilitates accurate analysis, it is, therefore, necessary to increase the amount of H_2O in the starting material with decreasing temperature (Tables 1 and 2). The final hydrous and anhydrous starting material compositions are presented in Table 2.

Experimental technique

Arc-welded gold capsules of 2·3 mm outer diameter containing the starting material were placed in an end-loaded, 1·27 cm piston-cylinder apparatus using a 'low-friction' and 'dry' furnace assembly, assembled from Teflon foil, a salt outer sleeve, Pyrex glass, a graphite heater and MgO inserts. Some experiments were also run without the Pyrex glass to test if the glass introduces some friction at low-*T*, high-*P* conditions. No systematic difference was observed, indicating that friction was fully released during the long duration of the experiments. In some experiments (labelled 'a' in Table 1), two gold capsules with different compositions (one carbonate-bearing) were run in one assembly. Temperature was controlled using type-B thermocouples ($Pt_{94}Rh_6/Pt_{70}Rh_{30}$) and is accurate to ±10°C. Pressure is converted from load and is accurate to 0·1 GPa. For the 4·5 GPa experiments, the assembly was initially held at 700°C, 3·5 GPa, for 2 h to allow the vessels and assembly to compact. In the 4·5 GPa experiments piston travel was monitored throughout the duration of the experiments. Minimal piston travel after 30–40 h indicates that friction has been released. The use of the 'dry' furnace assembly, gold capsules and the relatively low temperatures of the runs produces conditions close to the Ni–NiO transition (W. O. Hibberson, personal communication). Hydrogen loss from the glass or alloying of Fe with the gold capsule would potentially yield more oxidized mineral assemblages containing acmite and andradite components in pyroxene and garnet, respectively. Normalization of the experimental run products (see the Electronic Appendix, available for downloading from http://www.petrology.oxfordjournals.org) did not provide evidence for any significant acmite and andradite component, which suggests that no significant hydrogen loss occurred.

Diamond traps

For experiments with diamond traps we used 3·5 mm diameter gold capsules that were filled first with 18 mg of 40–60 μm diamonds as a fluid trap, followed by 65 mg of the hydrous starting material containing 6·8 wt% H_2O.

Table 1: Experimental conditions and run products

Run no.	*P* (GPa)	*T* (°C)	*hours*	wt% H_2O	Phases
C-2098D	2·5	600	168	6·8	**Am**, **Phe**, **Qtz**, *Rt*, *All*, *Ap*
C-1866a	2·5	700	183	6·6	**Am**, **Phe**, **Qtz**, *Rt*, *All*, *Ap*, *Gl*?
C-2099D	2·5	700	168	6·8	**Am**, **Phe**, **Qtz**, **Gl**, *Rt*, *All*, *Ap*
C-2246*	2·5	750	168	6·8	**Grt**, **Am**, **Qtz**, **Phe**, **Bt**, **Gl**, *Rt*, *All*, *Zir*, *Ap*
C-1846a	2·5	800	166	6·8	**Grt**, **Am**, **Qtz**, **Phe**, **Bt**, **Gl**, *Ky*, *Rt*, *All*, *Zir*, *Ap*
C-1928a	2·5	900	190	2·0	**Grt**, **Cpx**, **Qtz**, **Kfs**, **Bt**, **Gl**, *Rt*, *Ky*, *Mon*, *Zir*
D-48	3·0	850	284	3·4	**Grt**, **Cpx**, **Coe**, **Phe**, **Gl**, *Ap*, *Rt*, *Mon*
C-2082D	3·5	600	144	6·8	**Ctd**, **Cpx**, **Coe**, **Phe**, Q, *Ap*, *Rt*, *All*, *graph*
C-1857a	3·5	700	163	6·6	**Grt**, **Cpx**, **Coe**, **Phe**, Q, *Ky*, *Rt*, *All*, *Ap*
C-2083D	3·5	700	144	6·8	**Grt**, **Cpx**, **Coe**, **Phe**, Q, *Ap*, *Rt*, *All*, *Zir*
C-2247*	3·5	750	168	6·8	**Grt**, **Cpx**, **Coe**, **Phe**, **Gl**, *Ap*, *Rt*, *All*, *Mon*, *Zir*
C-1848a	3·5	800	168	6·8	**Grt**, **Cpx**, **Coe**, **Phe**, **Gl**, Ky, *Ap*, *Rt*, *Mon*, *Zir*
C-1578a	3·5	900	164	6·1	**Grt**, **Cpx**, **Coe**, **Gl**, Phe, Ky, *Ap*, *Rt*, *Mon*, *Zir*
C-1699a	3·5	900	260	3·1	**Grt**, **Cpx**, **Coe**, **Phe**, **Gl**, *Ky*, *Ap*, *Rt*, *Mon*
C-1867a	3·5	950	170	2·0	**Grt**, **Cpx**, **Coe**, **Phe**, **Gl**, Ky, *Rt*, *Ap*, *Mon*
C-2097D	4·5	700	168	6·8	**Grt**, **Cpx**, **Coe**, **Phe**, Q, Ky, *Ap*, *Rt*, *All*
C-2590*	4·5	750	144	6·8	**Grt**, **Cpx**, **Coe**, **Phe**, Q, *Rt*, *All*, *Ap*
C-2596*	4·5	800	120	6·8	**Grt**, **Cpx**, **Coe**, **Phe**, Q, *Ap*, *Rt*, *Mon*, *Zir*
C-1872a	4·5	800	162	6·8	**Grt**, **Cpx**, **Coe**, **Phe**, **Gl**, Ky, *Ap*, *Rt*, *Mon*, *Zir*
C-1614a	4·5	900	75	6·8	**Grt**, **Cpx**, **Coe**, **Phe**, **Gl**, Ky, *Rt*, *Mon*, *Zir*
C-1563a	4·5	1000	138	2·8	**Grt**, **Cpx**, **Coe**, **Gl**, Phe, *Ky*, *Rt*, *Mon*, *Zir*
C-1868a	4·5	1050	120	2·0	**Grt**, **Cpx**, **Coe**, **Gl**, Ky, *Rt*, *Ap*

Phases in bold have a modal abundance of >5%, phases in regular font have a modal abundance between 5 and 1%, and phases in italics are accessory phases. Experiments with suffix 'a' were run in assemblies containing two capsules; suffix 'D' indicates experiments with a diamond trap. Am, amphibole; Phe, phengite; Qtz, quartz; Coe, coesite; Grt, garnet; Bt, biotite; Gl, glass; graph, graphite; Kfs, K-feldspar; Ctd, chloritoid; Cpx, clinopyroxene; Ky, kyanite; Rt, rutile; All, allanite; Ap, apatite; Mon, monazite; Q, quench material from fluid; Zir, zircon.
*Experiments where no Pyrex sleeve was used.

The length of the fully loaded capsule was about 7 mm; this was placed in the hotspot of a 30 mm long MgO–graphite–Pyrex–NaCl assembly with the diamond trap located close to the thermocouple. Following each experiment, the gold capsule was pierced and dried to precipitate the remaining solutes in the fluid. In the experiments of Spandler *et al.* (2007*b*) performed with an identical starting material, the fluid was analysed for major and trace elements after the experiment. The fluid contained <0·3 wt% Na_2O and <0·05 wt% K_2O. It is expected that the vapour coexisting with such a fluid contained considerably less of these elements. Hence, the major and trace element content of the escaping vapour is at least an order of magnitude lower than that of the fluid phase at the *P* and *T* conditions of the experiments and therefore is considered to be negligible. The capsule was then opened at the end containing the diamond trap and the diamond aggregate was extracted. The diamond trap was either powdery (Fig. 2a) or cemented together (Fig. 2b). The diamonds and accompanying quench material were subdivided into three fractions taken at different distances from the residue (Tenthorey & Hermann, 2004). Fraction 1 was sampled from the uppermost section of the diamond trap, fraction 2 from the intermediate part and fraction 3 from the part of the diamond trap that was in contact with the pelite residue. A small sample of each fraction was mounted on a glass slide and covered by immersion oils. Optical inspection of these samples with a polarized light microscope allowed distinction between isotropic amorphous quench material and anisotropic hydrothermal minerals that formed by solution precipitation reactions during the relatively long experimental runs. Fraction 3 always contained significant amounts of minerals, whereas fraction 2 was dominated by amorphous quench and contained less than 5 vol.% of minerals. Only in the experiment at 2·5 GPa, 600°C, was the overall amount of minerals higher in all fractions. Interestingly, fraction 1 generally contained more precipitated minerals than

Table 2: Composition of the anhydrous and hydrous starting material (EPSM) and of experimentally produced glasses normalized to 100% anhydrous

Exp.:	EPSM	EPSM	2246	1846	1928	D29	2247	1848	1578	1699	1867	1872	1614	1563	1868
P (GPa):			2·5	2·5	2·5	3	3·5	3·5	3·5	3·5	3·5	4·5	4·5	4·5	4·5
T (°C):			750	800	900	900	750	800	900	900	950	800	900	1000	1050
SiO_2	68·83	64·15	73·43	74·59	71·32	72·72	74·87	73·77	73·57	73·18	72·24	72·72	72·31	70·66	68·72
TiO_2	0·67	0·63	0·21	0·17	0·25	0·31	0·27	0·31	0·35	0·44	0·43	0·46	0·55	0·60	1·03
Al_2O_3	14·70	13·70	14·47	14·90	17·26	15·32	13·56	13·78	14·43	14·85	15·02	12·32	13·63	15·21	14·91
FeO	4·67	4·35	0·89	0·78	0·65	0·81	0·62	0·88	0·88	0·77	1·12	0·93	0·94	1·04	1·29
MnO	0·11	0·10	<0·05	<0·05	<0·05	<0·05	<0·05	<0·05	<0·05	<0·05	0·06	<0·05	0·08	<0·05	<0·05
MgO	2·51	2·34	0·27	0·50	0·52	0·55	0·27	0·43	0·40	0·29	0·23	0·31	0·61	0·35	0·40
CaO	2·45	2·28	1·17	1·59	0·94	1·25	1·10	1·42	1·19	1·06	0·84	1·86	1·62	0·79	0·81
Na_2O	2·62	2·44	6·93	4·16	3·77	5·09	6·23	5·96	3·76	3·44	2·94	6·87	3·65	3·16	2·28
K_2O	2·94	2·74	2·61	3·39	5·09	4·06	3·08	3·29	5·19	5·76	7·01	4·45	6·37	7·93	10·05
P_2O_5	0·32	0·30	<0·20	<0·20	0·34	<0·20	<0·20	0·22	0·25	0·26	0·10	<0·20	0·29	0·26	0·49
Sum	99·8	93·01	99·97	100·08	100·14	100·10	99·99	100·07	100·01	100·06	100·00	99·91	100·05	100·00	99·98
Meas.			85·28	84·76	93·81	86·79	79·03	80·88	86·00	85·61	86·18	70·32	83·28	90·96	88·89
% melt			35	60	40	25	23	30	55	20	26	21	40	35	30
H_2O wt%		6·8	16	10	5	10	25	20	11	11	6	29	16	8	6
K_2O/H_2O			0·14	0·30	0·97	0·37	0·09	0·13	0·42	0·47	1·10	0·11	0·33	0·91	1·57
X_{Mg}			0·35	0·53	0·59	0·55	0·43	0·46	0·45	0·40	0·27	0·37	0·53	0·37	0·36
ASI			0·89	1·12	1·29	1·02	0·87	0·86	1·03	1·07	1·08	0·63	0·86	1·00	0·93
Ab			75	57	49	60	70	67	48	44	37	63	42	36	24
An			7	12	7	8	7	9	8	7	6	9	10	5	5
Or			18	31	44	32	23	24	44	48	58	27	48	59	71

The measured total (Meas.) is given. The melt fraction (% melt) in each experiment and the water content of the melt has been estimated on the basis of mass balance. X_{Mg} refers to the Mg/(Mg + Fe) atomic ratio and ASI is the alumina saturation index Al/(Na + K + 2Ca). Percentages of albite (Ab), anorthite (An) and orthoclase (Or) components as used in Fig. 7 are also given.

fraction 2, indicating that the fluid in the diamond trap was circulating through the pelite residue to some extent. This observation also shows that special care needs to be taken to obtain meaningful data from diamond traps. The three fractions of the diamond trap were then mounted on sticky carbon tape and the residue was sectioned longitudinally and mounted in epoxy. Both the sectioned residue and the diamond trap material were then examined in detail with a JEOL 6400 scanning electron microscope (SEM) equipped with EDS. The main minerals precipitated in the trap were quartz and phengite although minor amounts of omphacite were also observed. All analytical results presented in this paper derive from fraction 2, which contained nearly pure amorphous quench.

Analytical techniques

The phase relations were obtained from detailed studies of backscattered electron (BSE) images. Mineral compositions were mainly determined using a JEOL 6400 SEM (Electron Microscopy Unit, ANU) with EDS operating at 15 kV and a focused beam of 1 nA. At such low beam current, no alkali loss occurs in phengite (Hermann & Green, 2001). Also, because of the high resolution, mixed analyses can be avoided. Garnets were also analysed by wavelength-dispersive spectrometry (WDS) for major elements and, in particular, for accurate determination of the minor elements P, Na, Ti and Mn. The WDS analyses were conducted using a Cameca SX-100 electron microprobe at the RSES, ANU, operating at 15 kV and a beam current of 20 nA. The comparison of major element concentrations between the SEM EDS and the electron microprobe WDS analyses showed excellent agreement. Major-element melt compositions were also analysed by EDS by scanning glass pools over an area of 5 μm × 10 μm. The scanning and the low beam current prevent destruction of the volatile-rich glass and permit accurate determination of the alkali elements (Hermann & Green, 2001).

Material from the diamond trap, mounted on carbon tape, was analysed for major and trace elements by

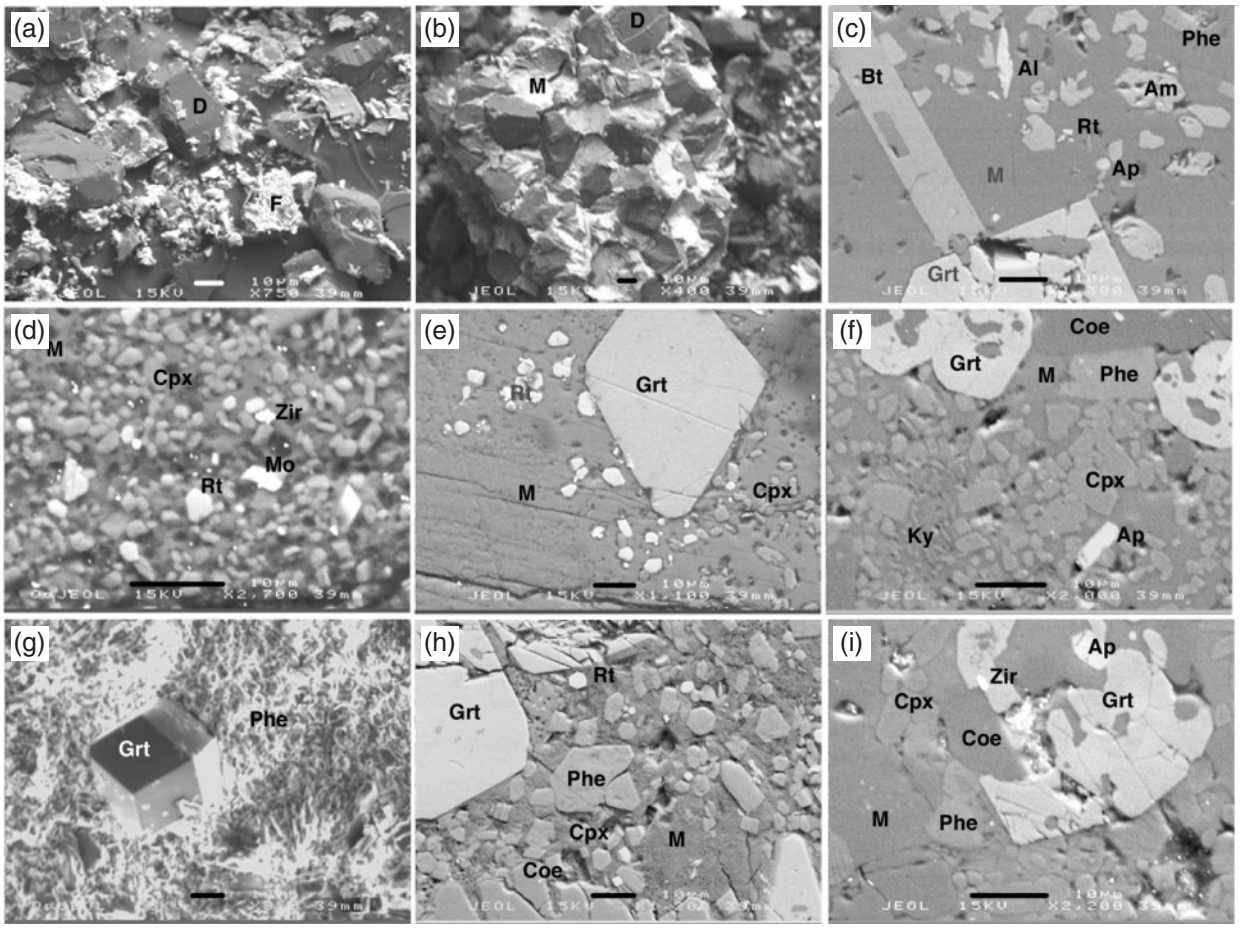

Fig. 2. Backscattered electron and secondary electron image (g) of experimental run products. For abbreviations see Table 1. F, quench products from aqueous fluid; D, diamond; M, melt (hydrous glass). Scale bar in all images represents 10 μm. (a) Powdery quench material in the diamond traps. (b) Diamonds from the trap are glued together by a hydrous melt indicating appearance of melt at 700°C, 2·5 GPa. (c) Hydrous melt coexisting with hydrous phases, garnet and accessory minerals. (d) Bubble-rich hydrous melt at 750°C, 3·5 GPa, coexisting with small crystals of clinopyroxene, rutile, monazite and zircon. (e) Large melt pools and idiomorphic garnet at 800°C, 3·5 GPa. (f) Phengite is still stable at 950°C, 3·5 GPa and is in textural equilibrium with the main assemblage garnet–kyanite–coesite–garnet–melt. (g) Idiomorphic garnet and fine-grained phengite at 700°C, 4·5 GPa; no glass. (h) The first appearance of bubble-rich hydrous glass at 800°C, 4·5 GPa with the typical high-pressure pelite assemblage. (i) Phengite is still present at 1000°C, 4·5 GPa; zircon and apatite have not melted out.

LA-ICP-MS at the Research School of Earth Sciences (ANU) using a pulsed 193 nm ArF Excimer laser with 100 mJ output energy at a repetition rate of 5 Hz (Eggins *et al.*, 1998) coupled to an Agilent 7500 quadrupole ICP-MS system. Laser sampling was performed in a He–Ar atmosphere. Data acquisition was performed by peak hopping in pulse counting mode, acquiring intensity data for each element during each mass spectrometer sweep. The sample stage was driven by a step motor, allowing continuous analysis along scans through the mounted material. Four scans per fraction were run using a spot size of 112 μm diameter with 25 sweeps of background followed by 80–100 sweeps of data collection. A synthetic glass (NIST 612) was used as external standard; reference values were taken from Pearce *et al.* (1997). Experiments were also doped with Cs in the hope of using this element as an internal standard as previously done in ultramafic (Tenthorey & Hermann, 2004) and K-free mafic systems (Kessel *et al.*, 2005*b*). However, the residual phengite in the experiments retained the great majority of the Cs and thus this technique did not provide satisfactory results. Because no reliable internal standard is available for the aqueous fluids absolute solubilities could not be directly determined. However, element ratios can be accurately determined with this method.

RESULTS

Phase relations

Phase relations were examined in detail by SEM (Fig. 2) and results are summarized in Table 1 and Fig. 3. In runs where glass is present experimental mineral phases are

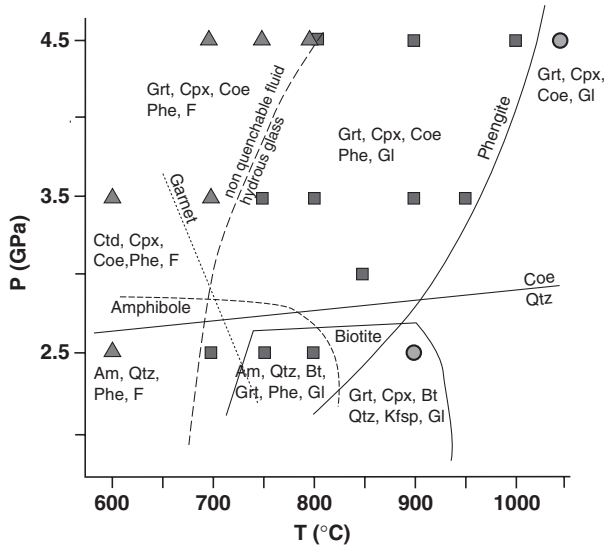

Fig. 3. *P–T* stability fields of different parageneses of the main minerals in subducted pelites. It should be noted that water contents vary between experiments (Table 1). The approximate stability limits of key phases are indicated. Triangles refer to runs where hydrous quench has been found. Glass and phengite are present in experiments shown by squares. Phengite has disappeared in experiments shown as circles. At sub-arc pressures the main solid assemblage in pelites consists of phengite–clinopyroxene–garnet–coesite and minor kyanite.

well crystallized and euhedral. The mineral grain sizes are in the range 20–100 μm for garnet and some coesite, 10–20 μm for other major and minor phases, and <10 μm for accessory phases. In experiments where hydrous quench was present, the phases had significantly smaller grain sizes and were more difficult to analyse.

Solid phases

At 2·5 GPa phase relations are complex with the phase assemblage changing over small temperature intervals. The assemblage is dominated by hydrous phases. At 600°C amphibole, phengite and quartz are the major phases and they coexist up to at least 800°C. Biotite and garnet appear at 750°C (Fig. 2c). At 900°C K-feldspar and clinopyroxene appear at the expense of phengite and amphibole, respectively, whereas biotite is still stable (Fig. 3). At the higher investigated pressures, phase relations are simpler. The assemblage garnet, clinopyroxene, coesite, phengite and minor kyanite is stable over nearly the entire range of investigated *P–T* conditions (Fig. 2f, h and i). Only at 700°C, 3·5 GPa, is chloritoid present instead of garnet. Phengite is stable up to 950°C at 3·5 GPa (Fig. 2f) and breaks down between 1000°C and 1050°C at 4·5 GPa (Fig. 2i). Kyanite is a minor phase in almost all experiments.

Rutile is the stable accessory Ti phase over the entire investigated *P–T* range. Apatite is also found in all experimental charges. Allanite is present at 2·5 GPa up to 800°C (Fig. 2c), and at 3·5 and 4·5 GPa up to 750°C. At higher temperatures monazite is stable up to 1000°C. Only at the highest conditions of 4·5 GPa, 1050°C was monazite not found. Zircon grains are very small and difficult to detect, but zircon has been observed in nearly all experiments. It is definitely present up to 900°C at 2·5 and 3·5 GPa and up to 1000°C, 4·5 GPa (Fig. 2i).

Fluid phases

The water added to the experiments always exceeded the capacity of the hydrous phases to store H_2O, resulting in the presence of a fluid phase in all experiments. At the higher investigated temperatures this fluid phase quenched to a hydrous glass, which indicates that a hydrous melt was present. The added water content was always lower than that required to obtain vapour-saturated melting for the given pressure range (Huang & Wyllie, 1981), and thus the experiments constrain fluid-present, vapour undersaturated melting in subducted sediments. No mineral quench phases have been observed within experimentally produced glass.

At 2·5 GPa, clean bubble-free glass was observed down to temperatures of 750°C (Fig. 2c). In experiment C-1866 at 700°C, 2·5 GPa no glass pools were observed. However, the experimental phases were well cemented together, as was generally observed in charges where glass is present. In a repeat experiment, a diamond trap was added to the starting material (C-2099D) to facilitate separation of fluid from solid phases. After opening the capsule, the diamond trap could be extracted as a coherent block. Inspection of the diamond trap under the SEM revealed that the diamonds were cemented together by a hydrous glass (Fig. 2b). In contrast, at 600°C, 2·5 GPa, the diamond trap after the experiment was powdery and appeared very different under the SEM (Fig. 2a). A very fine hydrous quench powder, which is not stable under the electron beam, was found. These observations indicate that at 600°C a solute-rich aqueous fluid was present, whereas at 700°C there was a hydrous melt.

At 3·5 GPa hydrous glass is present in experiments down to temperatures of 750°C (Fig. 2d). At 900 and 950°C the glass is bubble free, whereas at 800 and 750°C bubbles are abundant in the glass (Fig. 2e). At 700°C (C-1857) fine-grained minerals were observed, the grains were loose and significant porosity was present in the charge, indicative of an aqueous fluid during the run. To further test this hypothesis, a diamond trap experiment was run at the same conditions (C-2083D). The diamond trap showed the same characteristics as observed at 600°C, 2·5 GPa, indicating the presence of an aqueous fluid. At 600°C, 3·5 GPa the diamond trap again contained fine-grained, amorphous hydrous quench material.

At 4·5 GPa a hydrous glass was observed from 1050°C down to 800°C. The glass in the 1050 and 1000°C runs is bubble free. A small amount of bubbles appears in the 900°C experiment and a significant amount of bubbles

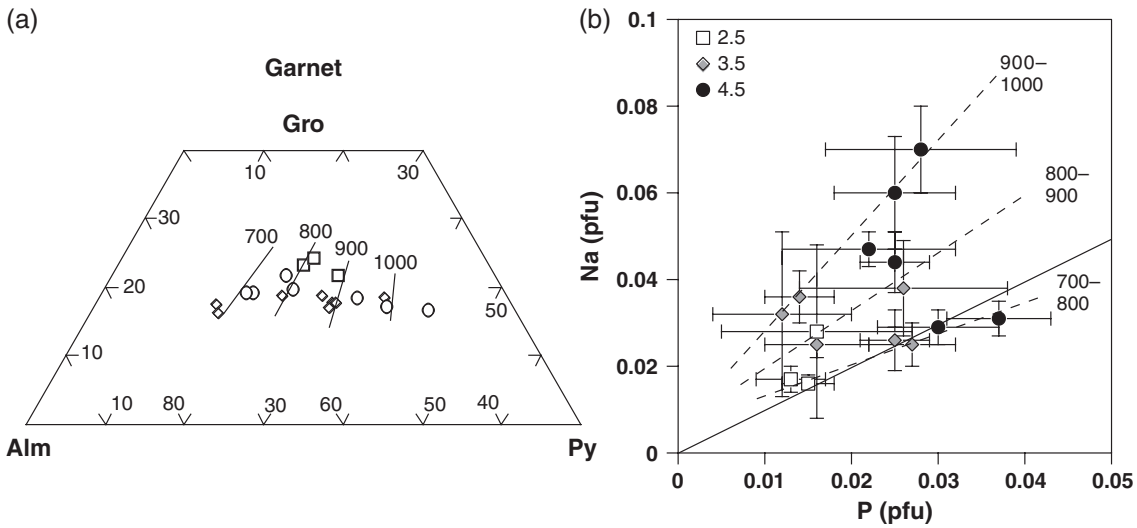

Fig. 4. (a) Garnet compositions plotted in molecular proportions of grossular (Gro), almandine (Alm) and pyrope (Py) show a strong increase in pyrope content with increasing temperature (numbers in°C). There is a slight decrease in grossular (Gro) content with increasing pressure (□, 2·5 and 3 GPa; ◇, 3·5 GPa; ○, 4·5 GPa). (b) Variation of Na and P (in cations per formula unit) in garnet from all experiments. At low temperature (700–800°C) the data plot on a 1:1 line. At higher temperatures there is more Na than P. Error bars refer to 1σ standard deviation of multiple analyses.

is present in the 800°C experiment (Fig. 2h). This suggests that some aqueous fluid exsolved during quenching from a melt that contained high water contents. In a second experiment at 800°C (C-2596), no glass pools were found. This might be related to the fact that the first experiment was run with two capsules, which produced a slight hot-spot, in which the melt pooled. At 750°C the run products were fine-grained and the charge was not well cemented. A Si-rich hydrous quench was observed in pores between mineral phases. The experiment at 700°C contained a diamond trap and the residual minerals were generally fine grained and not well cemented (Fig. 2g). Examination of the trap after the experiment revealed the presence of a powdery, amorphous quench material, similar to runs 2099D and C-2083D. From all these observations we suggest that the transition from quenchable hydrous glass to non-quenchable solute-rich fluid occurs at ~800°C at 4·5 GPa.

Phase compositions

The average composition of all analysed phases in the experiments is given in the Electronic Appendix (http://www.petrology.oxfordjournals.org)

Garnet

Large idomorphic garnet is generally slightly zoned. The cores are characterized by high TiO_2 contents (often ≥1 wt%) and by slightly higher MnO and CaO contents, whereas the MgO content is generally lower than in the rim. The following discussion is based on rim compositions, which are interpreted to be in textural equilibrium with the other phases. The most prominent feature in garnet is the increase of pyrope content with increasing temperature (Fig. 4a). Grossular contents decrease slightly with increasing pressure. The cation sum of garnet when normalized with all iron as ferrous iron is within error of 8·0, indicating that there are insignificant amounts of ferric iron. There is no evidence for supersilicic garnet [Si > 3 cations per formula unit (p.f.u.)] in any of the experiments. An interesting feature of the garnet compositions is the relatively high amounts of minor elements such as TiO_2, P_2O_5 and Na_2O; elements that are buffered in the experiments by coexisting rutile, apatite and omphacite, respectively. In all analysed garnets the TiO_2 content varies between 0·4 and 0·9 wt%. Generally, the TiO_2 content increases with increasing temperature. P_2O_5 contents range from 0·2 to 0·56 wt% and increase with increasing pressure. Na_2O was detected in all garnets and ranges from 0·1 to 0·5 wt%. Na_2O increases with pressure and temperature. Figure 4b displays the variation of Na vs P cations (p.f.u.) contoured with the experimental conditions. At 700–800°C, Na and P (p.f.u.) values plot on a 1:1 line indicating that at these conditions these elements enter garnet via a coupled substitution $NaPM^{2+}_{-1}Si_{-1}$. At higher temperatures, Na (p.f.u.) is much higher than P (p.f.u.) and thus Na must be incorporated by other substitutions such as $NaTi^{[o]}M^{2+}_{-1}Al_{-1}$. Some of the Ti might also be accommodated by the coupled substitution $Ti^{[o]}Al^{[T]}Al^{[o]}_{-1}Si_{-1}$.

Clinopyroxene

Clinopyroxene generally forms small grains that are difficult to analyse. It often exhibits zoning in FeO, with higher contents in the core than in the rim. Because of the small grain size it has not always been possible to analyse

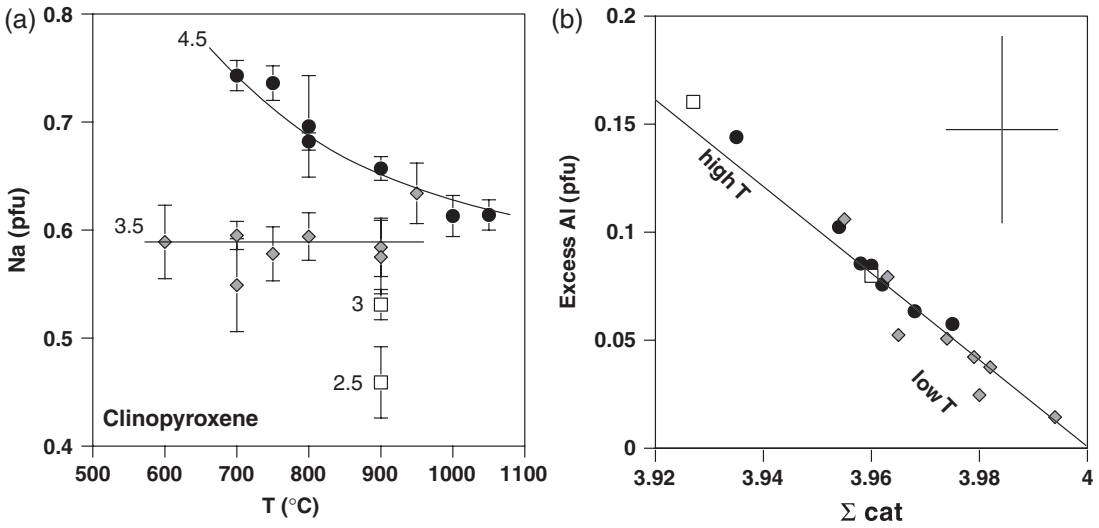

Fig. 5. (a) Na per formula unit in clinopyroxene as a function of temperature and pressure. (b) Excess Al (Al neither bound in a jadeite nor Ca-tschermakite component) vs cation sum indicates the presence of a Ca-eskaloite component in clinopyroxene. Error bars refer to 1σ standard deviation of multiple analyses. Symbols as in Fig. 4.

the rim only. The average analyses presented in the Electronic Appendix are based preferentially on rim compositions. Clinopyroxene is omphacitic in composition in all experiments. The jadeite component strongly increases with increasing pressure and reaches a maximum of 74% at 700°C, 4·5 GPa (Fig. 5a). At 3·5 GPa the jadeite content is nearly constant over the entire investigated temperature range. In contrast, at 4·5 GPa the jadeite content decreases significantly from 700 to 1050°C (Fig. 5a). TiO_2 content ranges from 0·1 to 0·6 wt% and generally increases with increasing temperature and decreases with increasing pressure. In some omphacite grains K_2O was detected when analysed by WDS; however, the rather large variation indicated that the analyses were affected by contamination from neighbouring phengite. In fact, when omphacite was analysed by SEM using a finer beam and a lower beam current, K_2O was always below the detection limit of ~0·2 wt%. All omphacite analyses exhibit Al > Na (p.f.u.). Therefore, no ferric iron is required to charge balance Na. The excess Al, which is not bound in a jadeite ($NaAlSi_2O_6$) or a Ca-Tschermak's ($CaAl_2SiO_6$) component, provides evidence for the presence of a Ca-eskolaite ($Ca_{0.5}\square_{0.5}AlSi_2O_6$) component in the omphacite. Because Ca-eskolaite contains a vacancy, it is expected that the sum of the cations should decrease with increasing Ca-eskolaite component. Figure 5b displays the correlation between excess Al and the sum of cations in relation to the theoretically expected line. The good agreement provides evidence that the experimentally produced omphacite contained up to 15% eskaloite component. The Ca-eskaloite component increases mainly as function of increasing temperature and does not change systematically with pressure. This is in good agreement with a recent comprehensive experimental study of Konzett *et al.* (2007), who reported that the Ca-eskolaite component in the assemblage clinopyroxene–garnet–coesite–rutile increases with increasing temperature, but that no significant increase with pressure can be observed.

Phengite

Phengite grains are relatively large and easy to analyse. We preferred to analyse phengite by EDS using a low beam current and, where possible, a rastered beam. Under such analytical conditions, no K loss during the analysis occurred. Phengite displays a systematic change in the celadonite component [$KAlMgSi_4O_{10}(OH)_2$] with changing conditions. The Si content (p.f.u) increases with increasing pressure and decreasing temperature (Fig. 6a). An interesting feature is the systematic change in TiO_2 content. The highest TiO_2 content of 2 wt% has been measured at 1000°C, 4·5 GPa. Overall, TiO_2 increases strongly with increasing temperature and decreases slightly with increasing pressure (Fig. 6b). Na_2O was detected in all phengites and the paragonite component reaches 19% at the lowest pressure investigated. At higher pressure the paragonite component is typically between 4 and 8%. All phengites contain $Mg + Fe > Si - 3$, indicating that there is a biotite component present, as previously observed by Green & Hellman (1982). This biotite component is highest when phengite coexists with biotite (i.e. at 2·5 GPa) and at this pressure it increases with increasing temperature to reach more than 30% at 800°C, 2·5 GPa. Incorporation of Ti presumably on the octahedral site of phengite could either be charge balanced by substitution of Al for Si on the tetrahedral site or by a coupled substitution $M^{2+}TiAl_{-2}$ on the octahedral site. The first

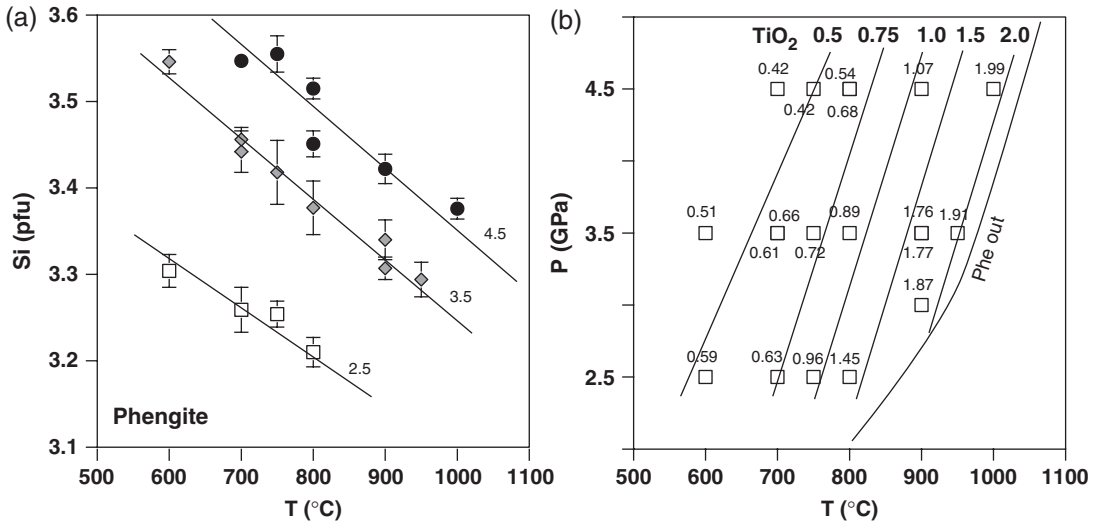

Fig. 6. (a) Si content of phengite as a function of pressure and temperature. Error bars refer to 1σ standard deviation of multiple analyses. (b) Contours of TiO_2 content (wt%) in phengite as a function of P–T grid. The high content of TiO_2 close to the phengite breakdown curve should be noted.

substitution produces phengite with a higher Al content, whereas the second substitution produces phengite with an Al content that is lower than would be expected for the celadonite and biotite substitution alone. We observe an Al deficit in all Ti-rich phengites, which indicates that Ti is dominantly incorporated by the $M^{2+}TiAl_{-2}$ substitution.

Other minerals

Only three runs at 2·5 GPa contained biotite. The TiO_2 content of biotite increases from 2 wt% at 750°C to 4 wt% at 900°C, whereas the FeO content significantly decreases over the same temperature interval. All biotites contain about 0·5 wt% Na_2O and are characterized by high Si content (p.f.u.) of 3·0. Four runs at 2·5 GPa contained sodic–calcic amphibole. With increasing temperature from 600 to 800°C, the Na_2O, SiO_2 and FeO contents decrease, whereas the TiO_2, K_2O and Al_2O_3 contents increase. The Na^{M4} (when normalized to 23 oxygens) decreases from 0·98 p.f.u. (600°C) to 0·56 p.f.u. (800°C), the Na^{A} is approximately constant at 0·33 p.f.u., whereas the $Al^{[T]}$ increases from 1 to 1·5 p.f.u. Only one run at 900°C, 2·5 GPa contained K-feldspar with the composition $Or_{58}Ab_{39}An_3$. The K-feldspar also contains detectable amounts of FeO (0·25 wt%).

Hydrous glass (quenched melt compositions)

Table 2 presents the glass analyses normalized to 100% on an anhydrous basis, whereas the Electronic Appendix contains the originally measured element concentration data. All normalized melt compositions are broadly granitic with SiO_2 contents between 69 and 75 wt% and Al_2O_3 contents from 12 to 17 wt%. K_2O and Na_2O vary strongly as a function of temperature. Na_2O decreases from about 7 wt% to 2·3 wt% from 750 to 1050°C. K_2O is buffered in the melt by coexisting phengite up to temperatures of 1000°C at 4·5 GPa and increases from 2·6 wt% at 750°C to 10 wt% at 1050°C (Fig. 7a). Consequently, the K_2O/Na_2O ratio varies over about an order of magnitude (Fig. 7b). Melt compositions have low anorthite components and trend from trondhjemitic to granitic compositions with increasing temperature (Fig. 7c). Low-temperature melts are typically peralkaline (Table 2), whereas only one melt composition determined at 900°C, 2·5 GPa is clearly peraluminous. The low totals of the glass provide evidence that there is a significant amount of H_2O dissolved in the melt, in agreement with the occurrence of bubbles in the glass. Mass-balance calculations using the known starting material composition and the compositions of all phases in the runs (Electronic Appendix) allowed determination of the amount of melt in each experiment (Table 2). From the known amount of water in the starting material of each experiment (Table 1) and the amount of OH stored in hydrous phases (determined by mass balance), the H_2O content of the melt could also be calculated. The principal source of error in this approach derives from the amount of melt determined from mass balance, and this error can be significant, especially at very low melt fractions. Our experiments were designed to produce relatively high amounts (>20%) of melt in each experiment, which results in estimated uncertainties in the H_2O content of the melt of 10–15% relative at the lower melt fractions and of 5–10% relative at the higher melt fractions. Figure 7d shows the H_2O content of the melt as a function of pressure and temperature. The resulting H_2O isopleths are characterized by

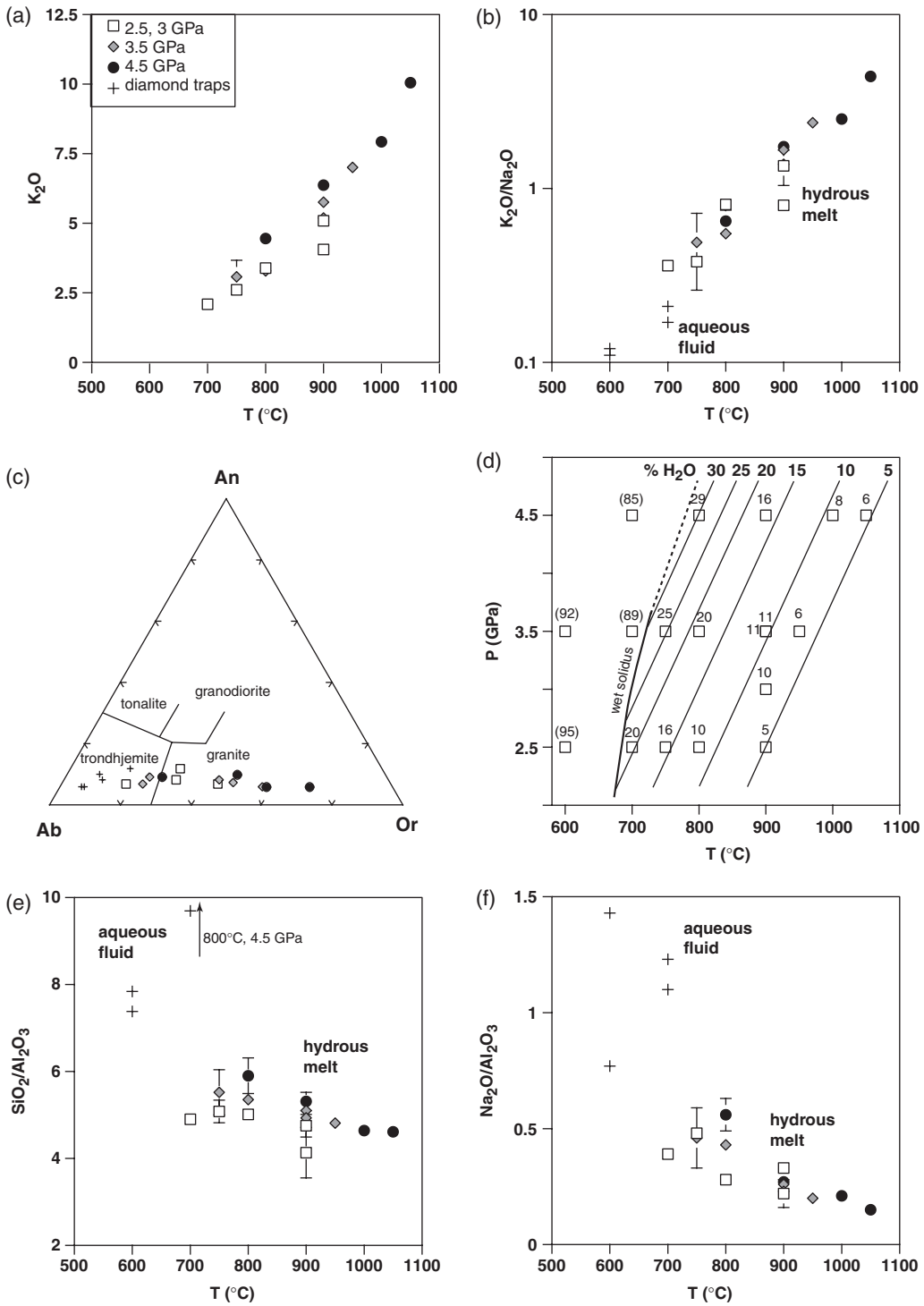

Fig. 7. (a) The K_2O content of melt is buffered by phengite in most experiments and increases systematically with increasing temperature. Pressure has no significant influence on the K_2O of the melt. (b) The ratio of K_2O to Na_2O increases over an order of magnitude from 600 to 1050°C. The significant difference between hydrous melts and aqueous fluids should be noted. (c) The aqueous fluid and the low-temperature melts are albite-rich, whereas the high-temperature melts are orthoclase-rich. All fluids are poor in anorthite component. Classification of silicic melts after Barker (1979). (d) Estimated water contents of hydrous melts in the experimental runs as a function of P and T and schematic contours of wt% H_2O in the melt. The numbers in parentheses represent rough estimates of the wt% H_2O of the aqueous fluid. The wet solidus is defined up to 3·5 GPa. Aqueous fluid and hydrous melt display distinctly different SiO_2/Al_2O_3 (e) and Na_2O/Al_2O_3 ratios (f).

Table 3: Composition of quench material in fraction 2 of the diamond traps determined by LA-ICP-MS

Exp.:	2099	2098	2082	2083	2097
P (GPa):	2·5	2·5	3·5	3·5	4·5
T (°C):	700	600	600	700	700
SiO_2	72·47	75·38	69·02	75·05	88·47
TiO_2	0·24	0·32	0·42	0·27	0·22
Al_2O_3	14·78	10·21	8·80	7·74	2·61
FeO	1·83	1·87	2·93	3·09	0·27
MnO	0·04	0·08	0·14	0·26	0·01
MgO	0·60	2·47	3·00	1·80	3·93
CaO	1·84	0·97	1·68	1·83	0·61
Na_2O	5·78	7·86	12·55	8·48	3·20
K_2O	2·09	0·83	1·46	1·47	0·69
Sum	100	100	100	100	100
H_2O	20	95	92	89	85
K_2O/H_2O	0·084	0·0004	0·0013	0·0018	0·0012
X_{Mg}	0·37	0·70	0·65	0·51	0·96
ASI	0·98	0·65	0·35	0·41	0·37
Alb	71	88	87	81	80
An	12	6	6	10	8
Or	17	6	7	9	11

Analyses are normalized to 100% anhydrous. The water content of experiment 2099 has been determined by mass balance. Other water contents are rough estimates based on published total solubilities in similar systems (see text for discussion). Other entities are as defined in Table 2.

a modest positive slope of 8°C/kbar. The highest amount of ~30 wt% H_2O was determined for the experiment at 800°C, 4·5 GPa. Fluids with higher amount of H_2O were not quenchable.

Diamond traps

To constrain the composition of the non-quenchable fluid phase, some experiments were run with diamond traps. Fraction 2 of the diamond traps contained more than 95% precipitates formed from the fluid during quenching. Therefore, this fraction was analysed by LA-ICP-MS to provide major element ratios in the quench material. The total sum of the major elements was then normalized to 100% (Table 3). Experiment 2099 provides a good test for the applied method. Detailed textural investigations showed that this trap contains hydrous melt rather than an aqueous fluid (Fig. 2b). The normalized values display all the characteristics of hydrous melts similar to the compositions reported in Table 2 and the data obtained plot along the trends established from where the melt pools have been directly measured. The quench materials in the other four low-temperature experiments have a significantly different major element composition from the hydrous melts, and are interpreted to represent quench from aqueous fluids. Whereas the SiO_2/Al_2O_3 value varies in a very limited range (4–6) in the hydrous melt, the aqueous fluids are characterized by much higher values (7–34; Fig. 7e). The aqueous fluid is also characterized by very high Na_2O and low K_2O contents, resulting in K_2O/Na_2O values that are much lower than those of the hydrous melts, but still consistent with the general temperature trend of this ratio (Fig. 7b). The relatively high Na_2O in conjunction with low Al_2O_3 makes the aqueous fluids strongly peralkaline. Therefore, Na_2O/Al_2O_3 is another effective ratio for distinguishing between aqueous fluid and hydrous melt compositions (Fig. 7f). Similar element ratios were reported for hydrous fluids trapped as synthetic fluid inclusions equilibrated at 2·2 GPa and 600–650°C by Spandler *et al*. (2007*b*); those results further support the validity of using these chemical criteria for distinguishing aqueous fluids from hydrous melt.

Element partitioning

The compositions of solid and fluid phases (Electronic Appendix) permit determination of the partitioning of major and minor elements among the phases present. Omphacite always contains higher Na than coexisting hydrous melts at all conditions investigated. The $D_{Na}^{Cpx/Melt}$ increases with pressure as well as with temperature from ~1·5 at 750°C, 3·5 GPa to ~4·5 at 1050°C, 4·5 GPa (Fig. 8a). Interestingly, in the two experiments where amphibole is present $D_{Na}^{Am/Melt}$ is below unity. The general affinity for Na_2O incorporation is omphacite > melt > amphibole > phengite > biotite > garnet. Because Na in garnet increases and Na in phengite decreases with increasing pressure and temperature, $D_{Na}^{Phe/Grt}$ is close to unity at 1000°C, 4·5 GPa. Ti is a minor element that can be detected in all major phases. The general affinity for TiO_2 incorporation is biotite > phengite > amphibole > garnet > melt ≥ omphacite. The Fe and Mg partitioning of coexisting minerals is best illustrated using $X_{Mg} = Mg/(Mg + Fe)$, which decreases in the following way: biotite > phengite > omphacite > amphibole > melt > garnet. Amphibole and omphacite have not been observed in the same run and the relative position is inferred from phengite–omphacite–melt and from phengite–amphibole–melt partitioning. An interesting observation concerns the X_{Mg} in coexisting garnet and melt. Generally the X_{Mg} in the melt is higher than in garnet. However, at 950°C, 3·5 GPa and at 1000°C, 1050°C at 4·5 GPa X_{Mg} of garnet is higher than in the melt. Such an inversion in the X_{Mg} is in excellent agreement with previous studies. Rubatto & Hermann (2007) found in an experimental study at 2 GPa that garnet has a lower X_{Mg} than the melt up to 950°C, at 950°C it is identical, and at 1000°C garnet has a higher X_{Mg} than the melt. Moreover, previous experiments by Green (1977) and Ellis (1986) showed that melts have a higher X_{Mg} than garnet below 1000°C at 3·0 GPa.

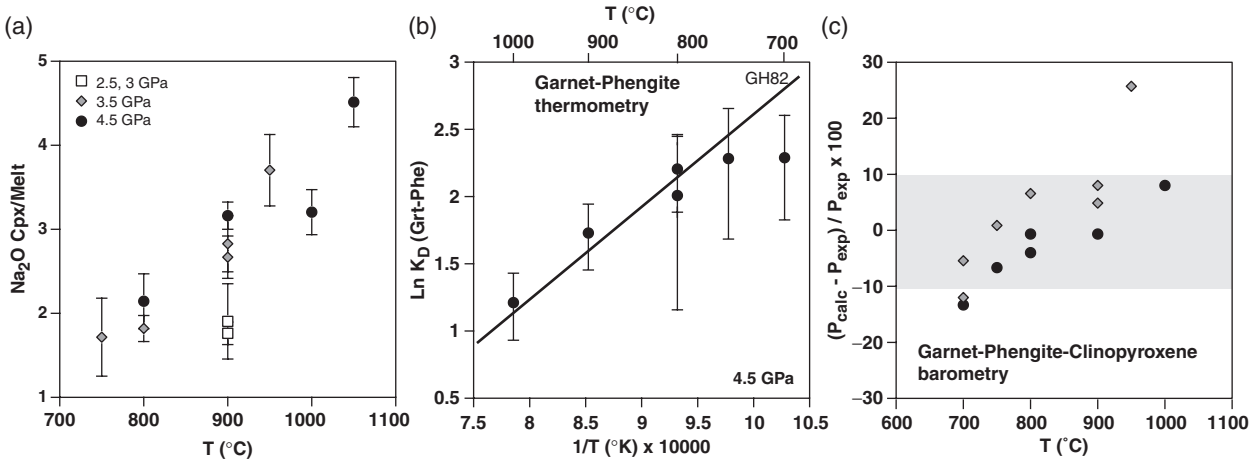

Fig. 8. (a) Na_2O (wt%) partitioning between clinopyroxene and melt as a function of pressure and temperature. It should be noted that clinopyroxene always contains higher Na_2O than the coexisting melt. (b) Fe–Mg partitioning between garnet and phengite at 4·5 GPa. $K_D = (Mg_{phe}/Fe_{phe})/(Mg_{grt}/Fe_{grt})$. The continuous line represents the formulated thermometer of Green & Hellman (1982) for a pelitic composition with high X_{Mg}. Error bars in (a) and (b) refer to propagated errors on the ratio from 1σ standard deviation derived from multiple analyses of the minerals. (c) Comparison between run pressures with calculated pressures at the given run temperature using the garnet–phengite–clinopyroxene barometer formulated by Krogh-Ravna & Terry (2004). The grey band refers to the estimated calibration error of the barometer. There is a very good match between calculated and nominal pressures in the temperature range 800–900°C. At lower temperatures, the calculated pressures are lower and at higher temperatures the calculated pressures are higher than the nominal run pressures.

It has long been known that the K_D of the Fe–Mg exchange in minerals is very sensitive to temperature (Ellis & Green, 1979; Green & Hellman, 1982). Figure 8b shows the variation of the Fe–Mg partitioning between garnet and phengite as a function of inverse temperature at 4·5 GPa. Data from lower pressure experiments have larger errors, so for simplicity these data are not plotted in the figure. Three important observations can be made from examination of the plot: (1) there is a clear trend in ln K_D with inverse temperature; (2) this trend is in very good agreement with the formulated thermometer of Green & Hellman (1982); (3) the propagated errors of the variability in analyses are rather large. Although there is also a general trend in garnet–clinopyroxene partitioning with inverse temperature, the large error in determining the FeO content in clinopyroxene because of zoning prevents a sensible test of garnet–clinopyroxene thermometers with the existing dataset.

DISCUSSION

The results of this experimental study provide information on two main aspects of research on the behaviour of deeply subducted sediments. The first part of the discussion addresses issues related to the use of ultrahigh-pressure (UHP) rocks as a natural laboratory for subduction processes. The second part focuses on the phase and melting relations in subducted sediments and how the nature and composition of the fluid phase determines the way these elements are recycled in the subduction factory.

UHP indicators in mineral compositions

It is not always easy to distinguish between minerals that formed at UHP conditions and minerals that formed or equilibrated during retrograde evolution. Most UHP rocks occur within subducted continental crust. Hence, detailed phase compositions in a pelitic starting material are useful to evaluate whether or not there are clear compositional signatures that can indicate a UHP origin of crustal rocks. Generally UHP conditions are deduced from the presence of coesite and/or diamond. In this section we compare the major and minor element composition of the main phases garnet and phengite in the experiments with data from UHP rocks as well as from deep-seated xenoliths to provide some constraints on possible UHP indicators in rock-forming minerals.

Garnet

The experimental garnets are characterized by high Na, Ti and P. At temperatures of 700–800°C the exchange $NaPM^{2+}_{-1}Si_{-1}$ seems dominant for the incorporation of P and Na. This exchange has been experimentally confirmed and a complete solid solution series has been documented at very high pressures (15–17 GPa) and high temperatures (Brunet *et al.*, 2006). In our experiments at temperatures higher than 800°C, a second substitution linked to Ti such as $NaTi^{[o]}M^{2+}_{-1}Al_{-1}$ is proposed to accommodate Na in excess of P. This substitution was first documented experimentally by Ringwood & Major (1971) at 5 GPa. Those workers also produced experimental garnets at 3·5 GPa and 1200°C with significant amounts of Na and Ti. Our results are in agreement with the conclusion of

Ringwood & Major (1971) that, in the presence of Ti, Na can enter garnet at relatively modest pressures. Previous experiments in the pressure range of 2·0–3·5 GPa in natural compositions suggested that Na, P and Ti are incorporated into garnet. Thompson (1975) conducted anhydrous melting experiments in basaltic compositions and found up to 0·4 wt% Na_2O, 0·6 wt% P_2O_5 and up to 3 wt% of TiO_2 in garnet. Auzanneau *et al.* (2006) investigated phase relations in a hydrous metagreywacke and reported garnet compositions with significant amounts of TiO_2 (~1 wt%) and 0·1–0·3 wt% of Na_2O in runs at 2·2–2·4 GPa, 800–900°C. In experiments on a natural tonalite composition, Patiño Douce (2005) found garnets with Na_2O ~0·1 wt% and TiO_2 >1 wt%, even at 1·5 GPa, 950°C.

Garnet grains in UHP rocks occasionally display exsolution of Ti-, Na- and P-rich phases, indicating that there was a P- and Ti-rich garnet precursor. Ye *et al.* (2000) found such garnets in the Sulu UHP belts of China, and Mposkos & Kostopoulos (2001) described similar garnet from the Rhodope UHP belt in Greece. By integrating the inclusions in garnet Ye *et al.* (2000) obtained 0·34 wt% Na_2O, 0·28 wt% P_2O_5 and 1·07 wt% TiO_2, and Mposkos & Kostopoulos (2001) obtained similar values of 0·6 wt% Na_2O, 0·33 wt% P_2O_5 and 1·03 wt% TiO_2. These values were used by both groups to postulate that the rocks originated from more than 200 km depth. However, the concentrations of these elements are very similar to what we find in garnet at 3·5–4·5 GPa (100–150 km equivalent depth), indicating that such compositions are not unequivocal proof of an ultra-deep origin of subducted crust.

According to our experiments and literature data, garnets with high Ti, Na and P should be the rule and not the exception in UHP terrains. However, it is interesting to note that most reported garnet analyses from UHP rocks display rather low concentrations of these minor elements. For example, garnet from diamond-bearing meta-granitic to meta-pelitic rocks from the Kokchetav massif and the Erzgebirge generally has TiO_2 <0·25 wt% and Na_2O <0·1 wt% (Zhang *et al.*, 1997; Massonne, 2003; Massonne & Nasdala, 2003). Only in some rare garnets from eclogites did Zhang *et al.* (1997) find some elevated TiO_2 contents of 0·34 wt% and Na_2O of 0·14 wt%. However, all these values are significantly lower than what is expected based on our experiments, given the diamond-facies metamorphic conditions of these rocks ($T = 950$–1000°C, $P \geq 4{\cdot}5$ GPa). This inconsistency between garnet compositions from experiments and natural UHP garnet compositions provides evidence that element re-equilibration occurred during exhumation. Such re-equilibration for P and Ti has been documented in UHP mafic rocks from the Northern Dabie Complex (Malaspina *et al.*, 2005). It is expected that garnet grains in crustal xenoliths are less affected by such retrograde modification. Although available literature data are restricted to mafic UHP xenoliths in which the buffering of P and Ti is not always clear, there is convincing evidence that garnet from such rocks contains much higher Na, P and Ti than is generally observed in UHP rocks of similar composition and metamorphic grade. For example, Sobolev & Lavrent'ev (1971) observed that Na_2O contents of 0·1–0·22 wt% are common in eclogitic garnet from diamond-bearing rocks, whereas 0·01–0·02 wt% Na_2O is generally present in garnet from UHP eclogite-facies rocks. Bishop *et al.* (1978) reported garnet compositions from eclogite xenoliths with up to 0·1 wt% P_2O_5, 0·14 wt% Na_2O and 0·8 wt% TiO_2.

In summary, there is clear evidence that garnet formed in subducted metapelitic rocks contains significant amounts of Na_2O, P_2O_5 and TiO_2. The much lower content of these elements in garnet from UHP felsic rocks indicates that, in most cases, garnet is not able to retain its original UHP chemical signature in such slowly cooling rocks. Garnet is one of the most important phases for thermobarometry. Therefore, the application of thermobarometers using garnet in relatively slowly cooled UHP rocks should be done with care, as in some cases these thermobarometers may be unable to provide meaningful constraints on peak metamorphic conditions.

Phengite

The Si content of phengite increases strongly with increasing pressure but depends also on the buffering mineral paragenesis, as has been demonstrated in several earlier studies (Massonne & Schreyer, 1987; Massonne & Szpurzka, 1997; Hermann, 2002*b*). The Si content of phengite must therefore be used in conjunction with the compositions of coexisting phases to estimate pressure. The most interesting observation on experimental phengite is the systematic change in TiO_2 content when buffered with rutile and quartz–coesite, a feature that has not been described before. The TiO_2 content increases strongly with increasing temperature and decreases moderately with increasing pressure (Fig. 6b), and provides a useful semi-quantitative tool to evaluate whether or not phengite compositions record peak conditions or equilibrated during exhumation. For example, Meyre *et al.* (1999) reported phengite containing 0·5–0·6 wt% TiO_2 from high-pressure pelites that experienced peak conditions of T ~650°C, P ~2·5 GPa. This is in very good agreement with the experimental values of 0·59 wt% TiO_2 (600°C, 2·5 GPa) and 0·63 wt% TiO_2 (700°C, 2·5 GPa). Phengite in metapelites of the Dora–Maira massif (peak conditions T ~730°C, P ~4 GPa) have ~0·4 wt% TiO_2 (Hermann, 2003), in good agreement with the measured 0·42 wt% TiO_2 in the experiment at 750°C, 4·5 GPa. Phengite-bearing eclogites of the Erzgebirge equilibrated at significantly higher temperatures of ~850°C with less precise pressure estimates of ~3·5 GPa (Schmädicke &

Müller, 2000). These phengites contain 1·1–1·5 wt% TiO_2, which again is consistent with our experimental results (Fig. 6b). Even higher TiO_2 contents in phengite of 1·75–2·04 wt% have been described from UHP metapelites of the Greenland Caledonides, for which peak metamorphic conditions of ~970°C and 3·6 GPa have been proposed (Lang & Gilotti, 2007). This is in very good agreement with the TiO_2 content of 1·9 wt% determined in an experiment at 950°C, 3·5 GPa. Because phengite breaks down at significantly lower temperatures of 700–750°C at crustal pressure (Vielzeuf & Holloway, 1988) than at UHP conditions (Fig. 3), phengite with such very high TiO_2 contents might be used as an indicator for UHP conditions. For phengites that do not contain a major biotite component (<20%), TiO_2 contents of >2 wt% seem to be stable only at pressures >3 GPa (i.e. at UHP conditions). In fact, such phengite has been observed as inclusions in zircon from the diamond-bearing gneisses of the Kokchetav massif (2·7 wt% TiO_2; Hermann *et al.*, 2001) and as inclusions in garnet from the Erzgebirge (3·3 wt% TiO_2; Massonne & Nasdala, 2003). These first results are promising; however, clearly more experimental data are needed to fully understand and quantify the TiO_2 incorporation in phengite as a function of pressure, temperature, bulk-rock composition and buffer paragenesis.

Implications for garnet–clinopyroxene–phengite barometry

Although the composition of single minerals, as discussed above, can give some insights into the conditions of potential UHP metamorphism, the most complete approach is to obtain pressure information by combining the composition of garnet, clinopyroxene and phengite. The compositions of these three phases are related through the fluid-absent, pressure-sensitive equilibrium

$$6\ \text{diopside}_{\text{cpx}} + 3\ \text{muscovite}_{\text{phe}} = 2\ \text{grossular}_{\text{grt}} + 1\ \text{pyrope}_{\text{grt}} + 3\ \text{celadonite}_{\text{phe}}. \quad (1)$$

The large stability field of garnet–phengite–clinopyroxene in a great variety of subducted crustal rocks makes this assemblage ideal for determination of pressure in UHP terrains (Carswell *et al.*, 1997; Krogh Ravna & Terry, 2004). In the following discussion we compare the calculated pressure at the nominal run temperature from phase compositions in experiments using the recently formulated garnet–phengite–clinopyroxene barometer of Krogh Ravna & Terry (2004) with the nominal pressure of the experimental runs (Fig. 8c). This barometer has been calibrated empirically and has so far not been tested by experiments. The calibration uncertainty at 3·5–4·5 GPa is ~10%, as indicated by the grey band in Fig. 8c. For most of the runs the pressure obtained from the barometer is within this grey band, indicating that it can be successfully used to identify UHP rocks. However, there is a clear trend in the data at 3·5 and 4·5 GPa, showing that the barometer is probably underestimating pressures at the low-temperature end (i.e. 700°C) and overestimating the pressures at the high-temperature end (i.e $T \geq 950$°C).

Pelite phase relations at sub-arc depths

The experiments of this study on a pelitic starting material document an important change in phase relations from fore-arc to sub-arc depth. There are complex phase relations in subducted sediments that involve a variety of hydrous phases at $P < 2{\cdot}7$ GPa (Patiño Douce & McCarthy, 1998; Hermann, 2002*b*; Poli & Schmidt, 2002; Auzanneau *et al.*, 2006). In our experiment this is manifested by the presence of amphibole, phengite and biotite at 2·5 GPa. Amphibole is stable only in runs at 2·5 GPa and below 900°C, as has also been found in experimental studies on mafic hydrous systems (e.g. Liu *et al.*, 1996; Poli & Schmidt, 2002). In contrast, the lack of garnet at 600 and 700°C, 2·5 GPa and at 600°C, 3·5 GPa is not consistent with natural phase assemblages or thermodynamic grids of high-pressure, low-temperature metapelites (Yardley, 1989; Powell & Holland, 1990) or other experimental studies. Experiments on pelitic compositions at 2–3 GPa by Nichols *et al.* (1994) produced garnet as part of the solid assemblage at temperatures down to 600°C. Spandler *et al.* (2007*b*), using the same starting compositions as used here, formed garnet in runs down to 600°C at 2·2 GPa. It should be noted, however, that in the experiments of Spandler *et al.* (2007*b*), garnet growth at subsolidus run conditions was achieved only by adding pyrope seeds to circumvent the sluggish nucleation of new garnet grains. Therefore, we expect that the lack of garnet in the lowest temperature experiments reported here is an artefact of sluggish nucleation of garnet at these conditions.

With increasing pressure from 2·5 GPa amphibole transforms to clinopyroxene and biotite reacts to form phengite. The transition from biotite-bearing to phengite-bearing parageneses has been investigated in detail by Auzanneau *et al.* (2006) in a greywacke bulk composition. They found that biotite disappears at 2·3–2·4 GPa at 800–900°C. At higher pressure, the paragenesis garnet + clinopyroxene + phengite + coesite ± kyanite is stable over a large P–T range (Fig. 9). Interestingly, this paragenesis is stable not only in metapelites but also in greywacke and K-bearing MORB (Schmidt *et al.*, 2004). This confirms that at sub-arc depths phengite will be the stable K phase in subducted crust. Within this dominant sub-arc paragenesis, a fluid-present melting reaction can be postulated based on the observed proportions and compositions of phases. Especially useful are those experiments in which the P–T conditions are constant, but the added water content changes. At 900°C, 3·5 GPa we performed two experiments with 6·8 and 3·1 wt% H_2O added. Based on mass balance using the compositions given in the Electronic Appendix,

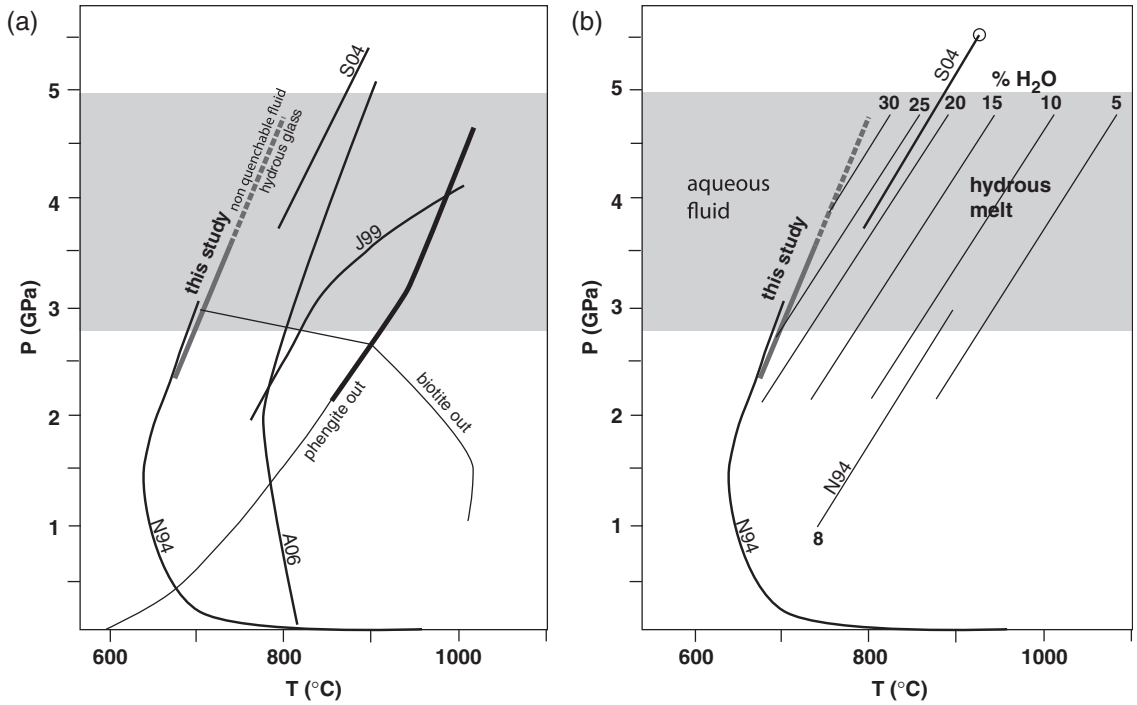

Fig. 9. (a) The positions of the wet solidus in metapelite and metagreywacke compositions in P–T space. Bold line: this study; N94, Nichols *et al.* (1994); J99, Johnson & Plank (1999); S04, Schmidt *et al.* (2004); A06, Auzanneau *et al.* (2006). The grey band indicates the pressure range of the subducted sediments at sub-arc depths. Also shown is the phengite-out curve determined in this study (bold line). The continuation to lower pressures is based on the experiments of Vieulzeuf & Holloway (1988). The approximate position of the disappearance of biotite is based on this study and the results of Auzanneau *et al.* (2006). (b) Water content of melts (in wt% H_2O) based on this study compared with results from Nichols *et al.* (1994). The fields of aqueous fluid and hydrous melts are shown. The solidus and the second critical endpoint (○) for pelites proposed by Schmidt *et al.* (2004) are also shown.

a significant decrease in the abundance of clinopyroxene, phengite and, to a lesser extent, coesite has been observed in the experiment with the higher water content, whereas there is a strong increase in the amount of melt and a smaller increase in the amount of garnet. These observations suggest the following melting reaction:

$$\mathrm{Cpx} + \mathrm{Phe} + \mathrm{Coe} + \mathrm{Fluid} \rightarrow \mathrm{Grt} + \mathrm{Melt}. \qquad (2)$$

Such a melting reaction has been proposed previously (Schmidt, 1996; Schmidt *et al.*, 2004) but is different from that of Auzanneau *et al.* (2006), who suggested that garnet is on the reactant side and not on the product side, which creates considerable problems in balancing Fe and Mg.

Phengite is stable to surprisingly high temperatures at sub-arc depths. At 3·5 GPa, it was still stable at 950°C, whereas at 4·5 GPa phengite disappeared between 1000 and 1050°C. Our experiments provide information on the minimum stability of phengite because we did not perform fluid-absent melting experiments. In fact, it has been observed in a natural tonalite composition (no fluid added, ~1 wt% H_2O) that phengite was stable up to 1010°C at 3 GPa and up to 1050°C at 3·2 GPa (Patiño Douce, 2005).

The new data in combination with literature data provide evidence for the key role of phengite as a K (and other LILE) carrier at sub-arc depths. Other trace elements are likely to be controlled by accessory phases such as apatite, zircon, rutile, allanite and monazite, which are stable to high temperatures and pressures (Table 1). The influence of accessory phases on the trace element contents of the liberated liquids will be presented elsewhere. The new data support previous suggestions that significant liberation of a range of trace elements is most probably related to fluid-present metamorphic conditions in the subducted sediments (Domanik & Holloway, 1996; Hermann & Green, 2001).

The position of the wet solidus

Experimental determination of the position of the wet solidus at low pressures (P <2·5 GPa) in felsic systems is relatively straightforward, as a clear transition from glass-absent to glass-present runs can be observed (Huang & Wyllie, 1981). For example, Spandler *et al.* (2007*b*) determined that the wet solidus for the same chemical system as investigated here is at 675°C at 2·2 GPa. However, at higher pressures, experimental determination of the solidus becomes more complex, as the amount of dissolved

H_2O in the hydrous melts at the solidus increases with increasing pressure (Huang & Wyllie, 1981). In this experimental set we found that the melt produced is quenchable to a glass only if the H_2O content is <30 wt% (Fig. 6a). Thus we are confident that we were able to track the wet solidus up to pressures of 3·5 GPa, where it is situated between 700 and 750°C. This is in very good agreement with the study of Nichols *et al.* (1994), who determined the wet solidus in subducted red clay sediments up to pressures of 3 GPa (Fig. 9). However, the wet solidus determined is very different from that in other studies. For example, Johnson & Plank (1999) reported a wet solidus in the red clay system that is more than 100°C higher than our results. This might be related to a difference in the starting material, because the red clay they used has significantly lower SiO_2 and higher FeO + MgO contents than the starting material used in the present study (Fig. 1), or to sluggish reaction in the lower temperature runs of their experiments because of the use of an already crystalline starting material. The locus of fluid-present melting for a metagreywacke composition (Auzanneau *et al.*, 2006), which is very similar in composition to our starting material (Fig. 1), is also at considerably higher temperatures (~100°C) at 3·5 GPa than the results of our study.

As pointed out above, at higher pressures we are only able to determine the transition from glass to non-quenchable fluid. From theoretical considerations of melting topologies it is evident that the wet solidus must have a steeper slope than the H_2O isopleths in the hydrous melt (Hack *et al.*, 2007). This means that, for the investigated system, the wet solidus should have a steeper slope than 80°C/GPa (Fig. 9). Interestingly, the proposed wet solidi of Schmidt *et al.* (2004) and Auzanneau *et al.* (2006) at P >3·5 GPa are very similar to the 25 wt% H_2O isopleth determined in this study (Fig. 9). It is important to note that these two studies were not well designed to trace the wet solidus. The amount of excess water in these experiments is very small and ranges from 0·4 wt% in the metagreywacke to 0·9 wt% in the metapelite. Considering that hydrous melts contain at least 25–30% of water at the wet solidus at P >3·5 GPa (Fig. 8b), this will result in extremely low melt fractions of 1–3%. Such low melt fractions are very hard to detect and virtually impossible to trace by mass balance. In contrast, in this study we have applied a different approach by increasing the water content at decreasing temperatures to keep the amount of melt produced high at about 20%. Such melt proportions are much easier to detect and provide larger pools for accurate analyses of the melt composition.

Composition of the fluid phase

The first-order control on the composition of the fluid phase is given by the H_2O content. Where the fluid phase is able to quench to a glass we classify it as a hydrous melt (Hermann *et al.*, 2006). For the studied pelite composition the transition from quenchable glass to non-quenchable fluid occurs at 30 wt% H_2O. With increasing temperature the H_2O content in the hydrous melt decreases in a systematic way (Fig. 9b). The liquidus determined by Nichols *et al.* (1994) for a red clay composition with 8 wt% H_2O is situated between the 5 and 10 wt% H_2O isopleths and thus is consistent with the isopleths determined in this study. At the low-temperature side of the solidus, the fluid phase is dominated by H_2O and thus represents an aqueous fluid (Fig. 9). In our study we were unable fully to quantify the amount of solute in the diamond traps. However, a comprehensive compilation of major element solubilities by Manning (2004) indicates that such aqueous fluids are surprisingly dilute and are likely to contain <5 wt% of total dissolved solutes at P <2·0 GPa and T ~600°C. At 2·2 GPa and 600–650°C, Spandler *et al.* (2007*b*) constrained the solubilities of elements with synthetic fluid inclusions using a starting material identical to that in this study. They found that total dissolved solutes range from ~4 to 5·5 wt%. This value is likely to be representative also for our run at 600°C, 2·5 GPa (Table 3). Solubilities tend to increase with increasing pressure and temperature (Manning, 2004), and guided by the general topology of the solubility isopleths (Hack *et al.*, 2007) we have estimated that the total dissolved solutes are ~8 and 11 wt% at 3·5 GPa at 600 and 700°C, respectively. This seems reasonable considering that Kessel *et al.* (2005*b*) reported total solute contents of ~12 wt% at 4·0 GPa, 700°C in the MORB + H_2O system. This system produced a mineral assemblage (apart from phengite) similar to that in the pelite system and, considering that the main solutes are SiO_2, Al_2O_3 and Na_2O (Table 3), total solute contents are likely to be comparable. For the run at 4·5 GPa, 700°C we estimated a total amount of solutes of 15% based on the findings of Kessel *et al.* (2005*b*) in the MORB + H_2O system; those workers reported aqueous fluids with total dissolved solutes of 7–17 wt% in the range 4·0–5·0 GPa and 700–800°C.

As solute contents increase along the solidus for the aqueous fluid and the H_2O increases in the hydrous melt, the two compositions merge together until they are the same at the second critical endpoint where the solidus terminates. The solubility isopleths obtained in this study indicate that at 3·5 GPa the second critical point has not been reached for the pelitic bulk composition. However, it must be noted that the design of our and the Schmidt *et al.* (2004) experiments is not suitable to detect any closure of the miscibility gap between aqueous fluid and hydrous melt. The position of the second critical endpoint cannot be determined with such experiments because the melts are no longer quenchable along the solidus above 3·5 GPa. It is necessary to conduct experiments at high and variable water contents to locate the second critical endpoint.

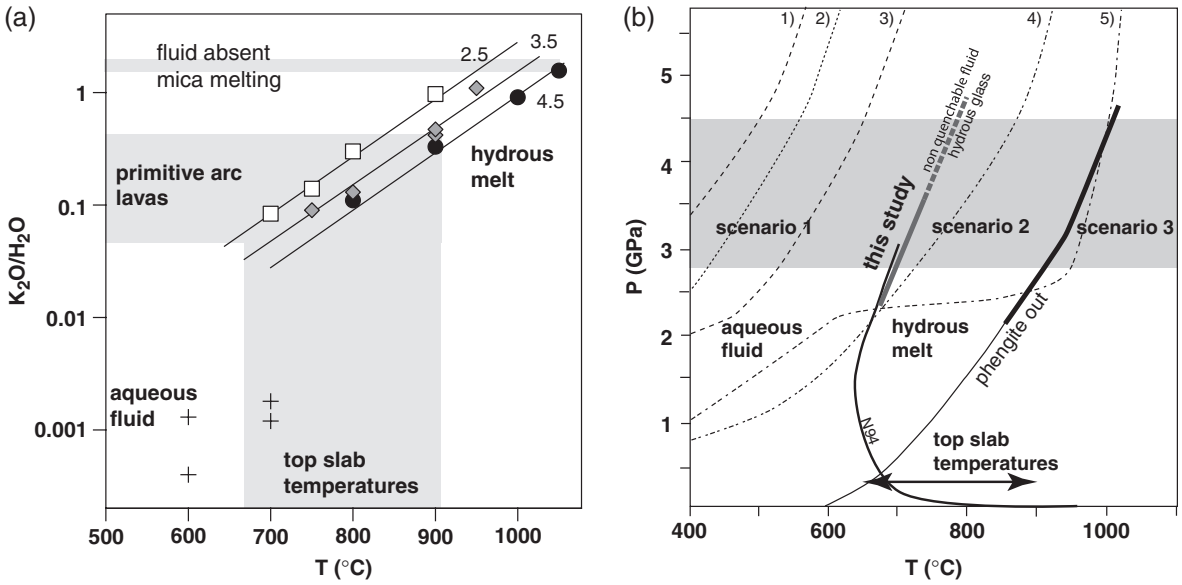

Fig. 10. (a) Variation of K_2O/H_2O in aqueous fluids and hydrous melts produced in the experiments compared with the range of K_2O/H_2O in primitive arc lavas and the K_2O/H_2O that would result from fluid-absent melting of phengite- or phlogopite-bearing rocks. (b) *P–T* diagram illustrating the three fundamentally different scenarios for element transfer in subduction zones when thermal models for top-slab temperatures are compared with the position of the wet solidus and the stability of phengite. In scenario 1, elements are transferred by an aqueous fluid; in scenario 2, by fluid-present melting; in scenario 3, by fluid-absent melting. Top-slab temperatures from numerical and analogue models: 1, 27° angle of subduction, 10 cm/year convergence rate, 50 Myr old oceanic crust; 2, 27° angle of subduction, 10 cm/year convergence rate, 20 Myr old oceanic crust; 3, 27° angle of subduction, 3 cm/year convergence rate, 20 Myr old oceanic crust; [numerical models 1–3 are from Peacock *et al.* (1994)]; 4, scaled analogue model: 49° dip, 3·5 cm/year convergence rate (Kincaid & Griffiths, 2004); 5, numerical model with enhanced coupling with the mantle wedge, 60° dip, 4·5 cm/year convergence rate, 10 Myr old oceanic crust (van Keken *et al.*, 2002).

As long as solubilities in the fluid phase are considered, the actual position of the second critical endpoint is not of paramount importance because there is a strong increase in solubilities over a temperature interval of ~100°C (as observed, for example, between 700°C and 800°C, 4·5 GPa) whether or not the wet solidus is still present (e.g. Manning, 2004; Hermann *et al.*, 2006).

The large melt pools obtained in this study permit accurate analysis of the experimental melts as a function of increasing temperature (Fig. 7). The melts are essentially granitic in composition. The most significant observed change within the granite field is the change of Na_2O and K_2O with temperature. Close to the wet solidus the melts are trondhjemitic with $Na_2O > K_2O$. At higher temperatures, the melts are granitic *sensu stricto* with $K_2O > Na_2O$. It is interesting to note that a very similar trend has been observed at lower pressures by Patiño-Douce & McCarthy (1998). Fluid-present melting in a muscovite schist at 700–750°C, 0·6–1·0 GPa produced trondhjemitic melt compositions, whereas melting at higher temperatures produced granitic melt compositions. This similarity in melt composition evolution with temperature at high and low pressures is not expected, as the buffering paragenesis changes significantly from quartz–plagioclase–muscovite–biotite–garnet (low pressure) to coesite–clinopyroxene–phengite–garnet (high pressure). Because of the large stability field of phengite, most experimental melts are buffered in K_2O. In fact, there is a systematic increase in K_2O with increasing temperature, as is expected for an element that has a constant composition in the buffering phase (Fig. 7a). In conjunction with the decrease in H_2O with increasing temperature, there is a very pronounced and systematic change of K_2O/H_2O as a function of temperature (Fig. 10a). Figure 10a is used to show how efficiently K_2O can be removed from subducted sediments as a function of temperature, nature of the fluid phase and available H_2O. At low temperatures an aqueous fluid is stable, and hence a very high fluid–rock ratio is needed to strip substantial K_2O out of subducted sediments. In contrast, at higher temperatures, much less H_2O is required to efficiently remove K_2O with a hydrous melt. Figure 10 can also be used to predict, in experiments with a given K_2O/H_2O, at which temperature it is expected that the solid K phase is completely dissolved in the produced fluid. The temperature range of phengite dissolution, used as an argument for the presence of supercritical fluids by Schmidt *et al.* (2004), can be readily explained in terms of this diagram. A K_2O/H_2O ~1·2 in their starting material is reached by the hydrous melt at 1000–1100°C, in agreement with the disappearance of phengite observed by Schmidt *et al.* (2004).

We have already highlighted the difficulties of constraining the nature of the fluid phase based on textural observations when the amount of fluid phase is low and/or the fluid phase does not quench to a glass. However, in this study we have observed some compositional characteristics that might help researchers in future studies to constraint the nature of the fluid phase. Element ratios are particularly useful, because determination of absolute concentrations is often difficult in the hydrous quench from aqueous fluids. We found that SiO_2/Al_2O_3 and Na_2O/Al_2O_3 abruptly increase from hydrous melts to aqueous fluids (Fig. 7e and f). This is in excellent agreement with the calculated solubilities in aqueous fluids in equilibrium with eclogite, showing that Si and Na are the main cations and Al is a minor component (Manning, 1998). The Na_2O/Al_2O_3 of aqueous fluids in equilibrium with a high-pressure metapelite has also been determined in fluid inclusions trapped in experiments at 2·2 GPa, 600–650°C and is close to unity (Spandler *et al.*, 2007*b*), in agreement with our data (Fig. 7f). Green & Adam (2003) analysed the quench material precipitated from aqueous fluids that had been equilibrated with a basaltic eclogite assemblage at 650–700°C, 3·0 GPa. The quench material was characterized by high SiO_2/Al_2O_3 of 12–20 and high Na_2O/Al_2O_3 of 0·7–0·8, providing further evidence for the distinct characteristics of these ratios in aqueous fluids.

A surprising feature is the very low K_2O content of the aqueous fluids, which is between 0·04 and 0·16 wt% when the H_2O content of the fluid is taken into account (Table 3). Such low K_2O contents have also been observed in the fluids present in the K-bearing basalt experiments of Green & Adam (2003). Although their starting material contained only 0·3 wt% K_2O and they applied a high H_2O/starting material ratio of unity, all experiments produced residual phengite. This provides strong evidence that the solubility of K_2O in the aqueous fluid must be smaller than 0·3 wt%. In fact, if the K_2O content of the fluid is normalized to a total solute content of 5 wt%, as suggested by Green & Adam (2003), then it reaches values of 0·07–0·11 wt%; these values are in excellent agreement with the low concentrations found in our study.

Element recycling and top-slab temperatures

One of the most remarkable characteristics of primitive arc lavas compared with MORB is the distinct enrichment of H_2O and LILE (Tatsumi & Eggins, 1995). A range of isotopic and geochemical criteria provide strong evidence that these components are derived from the subducted slab (Hawkesworth *et al.*, 1993; Plank & Langmuir, 1993, 1998). Although the H_2O may be sourced from a number of lithologies in the slab (Poli & Schmidt, 2002), several studies have confirmed that subducted sediments play a key role in the LILE budget of subduction zones (Plank & Langmuir, 1993, 1998; Peate *et al.*, 1997). In particular, pelites are regarded as the most important component of the subducted sediment for hosting most lithophile trace elements (Plank & Langmuir, 1998). It is, therefore, of prime interest to understand the nature and composition of the fluid phase that is formed at sub-arc depths in subducted pelites. To evaluate the process of LILE recycling, it is necessary to compare the position of the wet metapelite solidus (and the extension of the transition of hydrous melt to non-quenchable fluid) to thermal models of top-slab temperatures. Figure 10b shows a variety of thermal models with respect to the wet pelite solidus, the field where hydrous melts are stable and the stability of phengite. Thermal modelling has shown that temperatures at the top of the subducting slab are mainly controlled by the age of the incoming plate (the older the cooler) and the speed of subduction (the faster the cooler (Peacock *et al.*, 1994). Recent thermal and mechanical modelling has also highlighted the importance of coupling between the slab and mantle wedge, which may dramatically influence temperatures on top of the slab (van Keken *et al.*, 2002; Kincaid & Griffiths, 2004). The variety of controlling parameters results in vastly different model conditions at sub-arc depths that range from very cold (400–600°C) to very hot (950–1000°C). This highlights the need to obtain independent constraints on top-slab temperatures.

To characterize recycling of elements from the subducted sediments to the mantle wedge, we can consider three fundamentally different scenarios. In the first scenario, the top-slab temperature is within the aqueous fluid field at relatively low temperatures at sub-arc depths. This is the case for all but the hottest proposed geotherms of the models given by Peacock *et al.* (1994). Under such conditions effective extraction of K_2O and other LILE will be difficult. Our experiments have shown that the K_2O content and, more importantly, the K_2O/H_2O ratio of such fluids are very low (Fig. 10a). This means that LILE can be removed by fluids only in zones where there is a very high fluid–rock ratio. Also, the solubility of LREE, which are often enriched in arc lavas, is extremely low (Hermann, 2002*a*; Spandler *et al.*, 2007*b*). In the second scenario, top-slab temperatures are high enough (>700°C) for fluid-present melting at sub-arc depths, but no fluid-absent melting of phengite occurs. Kincaid & Griffiths (2004) reported results from scaled analogue models that produced top-slab temperatures that fall within this scenario. K_2O and LILE will be efficiently removed from the sediments depending on the availability of an externally derived fluid that triggers melting. It has been suggested that the breakdown of hydrous phases in mafic and ultramafic rocks in the deeper and cooler parts of the slab might provide the fluids necessary for melting the sediments on top of the slab (Hermann & Green, 2001). Alternatively, hybrid chlorite- and talc-rich rock types that form as a result of interaction between the subducted slab and the mantle wedge might liberate significant amounts of

fluid at 700–800°C at sub-arc depths and thus will trigger melting of the sediments (Spandler *et al.*, 2007*a*). In the third scenario, very high top-slab temperatures of 950–1000°C might lead to fluid-absent melting of phengite in subducted sediments. Such high top-slab temperatures could occur where there is enhanced coupling with a hot mantle wedge (van Keken *et al.*, 2002) or where asthenospheric inflow occurs in response to slab rollback (Kincaid & Griffiths, 2004). In such a case, nearly complete transfer of K_2O and LILE from the subducted sediments to the mantle wedge occurs at sub-arc depths independent of whether or not there is additional fluid fluxing.

One interesting aspect of fluid-present melting in sediments is that the amount of K_2O in the melt (buffered by phengite) increases systematically with increasing temperature. It was suggested previously that in many island-arc systems there exists a relationship between the K_2O content of primitive lavas and the depth to the top of the subducting slab beneath the volcano—the so-called '*K–h*' or 'potash–depth' relationship (Dickinson, 1975). Consequently, it has been postulated that pressure is the primary control on K_2O release from the slab. Our study, however, suggests that temperature and not pressure is the controlling parameter. Because the temperature at the top of the subducting slab increases with increasing depth, the observed 'potash–depth' relationship still holds.

We suggest that the systematic change in the K_2O/H_2O ratio in the slab fluid as a function of temperature and, to a lesser extent, pressure, provides a useful tool to distinguish between the three scenarios outlined above. K_2O is buffered by residual phengite and is a good proxy for the behaviour of the LILE, which are the most important elements in the subduction component of arc lavas. The rationale behind normalizing to the water content is that the amount of water added to the mantle wedge will be a principal factor in determining how much basaltic melt is produced during wet melting of the mantle wedge peridotite, which in turn will have an influence on the final concentration of LILE in the resultant arc magmas. The K_2O/H_2O of the fluid phase leaving the subducted sediments at the top of the slab is extremely low ($\ll$0·002) in scenario 1 (Fig. 10a). As soon as hydrous melts are present (scenario 2) the K_2O/H_2O increases drastically to 0·1–1 for the temperature range of fluid-present melting. For fluid-absent phengite melting at sub-arc depths, as outlined in scenario 3, the K_2O/H_2O is bracketed between ~1, given by the high temperature of melting, and ~2·3, given by the stoichometry of phengite (10·5 wt% K_2O, 4·5 wt% H_2O).

These constraints can now be compared with the K_2O/H_2O ratio of primitive arc lavas. Primitive lavas from a range of volcanic arcs have between 0·2 and 0·8 wt% K_2O (Kelemen & Hanghoj, 2003) and between 2 and 4 wt% H_2O (Sobolev & Chaussidon, 1996; Stern, 2002), giving K_2O/H_2O ratios of between 0·05 and 0·4. An excellent dataset has been recently published on melt inclusions in olivine from the Kamtchatka arc, where K_2O and H_2O have been measured in the same inclusions (Portnyagin *et al.*, 2007). The observed K_2O/H_2O values range from 0·05 to 0·42, with the majority of data clustering at 0·25. The depleted mantle source of arc magmas is expected to contain of the order of 0·007 wt% K_2O and 0·01 wt% H_2O (Salters & Stracke, 2004) and so is unlikely to contribute significantly to the budget of these elements in arc magmas. Therefore, we can reasonably assume that the K_2O/H_2O ratio of primitive arc magmas is primarily derived from slab contributions.

To make a link between the K_2O/H_2O of arc magmas and the K_2O/H_2O of the slab-derived sediment flux, we have to consider potential alteration of this ratio in the mantle wedge according to the three different scenarios. For models predicting cool top-slab temperatures (scenario 1), aqueous fluids leaving the slab will interact with the mantle wedge and form a variety of hydrous phases such as antigorite, amphibole, talc, chlorite and phlogopite (Poli & Schmidt, 2002). Talc, chlorite and phlogopite, in particular, are stable up to considerable pressures and temperatures and the formation of these phases will alter the H_2O and K_2O content of the residual fluid. However, overall it is expected that the solubilities in the peridotite system are lower than in the pelite system and that the residual fluids are likely to be H_2O-rich, aqueous fluids with very low K_2O/H_2O. An interesting alternative model is that the fluid, which transports the slab signature to the locus of partial melting in the mantle wedge, derives from the breakdown of the hydrous chlorite–talc assemblage, which will occur at ~800°C (Spandler *et al.*, 2007*a*). We can estimate the proportion of hydrous minerals from the interaction of peridotite with aqueous fluids derived from the subducted sediments. For a fluid composition such as that determined at 600°C, 3·5 GPa (Table 3), we obtain an estimated talc:chlorite: phlogopite ratio of 30:15:1. If upon dehydration of such an assemblage at 800°C all the K_2O hosted in phlogopite enters the fluid phase, the resulting K_2O/H_2O ratio would be ~0·03. This is a maximum value as potentially some phlogopite will remain. This calculated ratio is considerably higher than in the original aqueous fluid leaving the slab, but is still significantly lower than the K_2O/H_2O ratio in arc lavas (Fig. 10). Therefore, it is very difficult to explain the K_2O/H_2O of arc lavas with scenario 1. Clearly, more experiments are needed to constrain the solubility of K_2O in aqueous fluids in such systems.

In the second scenario a hydrous melt is produced from the subducted sediments. This melt will most likely enter the mantle wedge at pressures above the amphibole stability field (Fumagalli & Poli, 2005) and at temperatures

that exceed the stability of antigorite, talc and chlorite (Poli & Schmidt, 2002). Hence, the only mineral phase capable of altering the K_2O/H_2O is phlogopite. Sekine & Wyllie (1982) have shown that interaction of granitic melts with peridotite will generally produce phlogopite. The extent of phlogopite formation depends on the temperature and especially on whether the melts are in contact with olivine or are shielded by the formation of new orthopyroxene. Malaspina *et al.* (2006) have investigated garnet-orthopyroxenites that have been interpreted as the products of interaction of peridotites with hydrous silicate melts at sub-arc pressures. They have observed that a residual fluid was trapped in the garnet that was enriched in incompatible elements. These garnet-orthopyroxenites are surrounded by layers of phlogopite, which probably formed during the interaction process (N. Malaspina, personal communication, 2007). Phlogopite has K_2O/H_2O of ~2, given by the stoichiometry. Figure 10 shows that hydrous melts released from the slab at temperatures of 700–900°C have a K_2O/H_2O of 0·1–1, which is lower than the K_2O/H_2O of phlogopite. Thus if phlogopite is formed in the mantle wedge peridotite, this will lower the K_2O/H_2O of the residual fluid that will enter the locus of wet melting. The observed K_2O/H_2O of ~0·05–0·4 of primitive arc lavas thus constrains the likely minimum K_2O/H_2O in the slab-derived fluid phase. Therefore, estimated top-slab temperatures based on the K_2O/H_2O of arc lavas would represent minimum values, and would depend on the amount of interaction of the slab-derived fluid with the mantle wedge. In the case of channel flow, such interaction would be minimal and the slab signature could be transported nearly entirely to the locus of partial melting. In such a case K_2O/H_2O temperature estimates based on this work would be accurate. On the other hand, if the fluid is transported via porous flow, extensive interaction and phlogopite formation is expected. K_2O/H_2O would then be determined by the solubility of phlogopite in aqueous fluids in the peridotite system. No experimental results are available yet to quantify this process, but it is expected that K_2O/H_2O would increase systematically with increasing temperature.

Fluid-absent melting of phengite at high temperatures (scenario 3) produces melts that have virtually the same K_2O/H_2O as phlogopite. Therefore in such a case, the K_2O/H_2O is not significantly changed by the potential formation of phlogopite in the mantle wedge. It is also worth noting that fluid-absent melting of a phlogopite-peridotite would produce melts with K_2O/H_2O of ~2. These values are significantly higher than what is observed in primitive arc lavas and consequently we do not consider this scenario to be likely.

The combination of our experimental results on the systematics of K_2O/H_2O variation in the fluid phase released from subducted sediments with considerations of the interaction of these fluids with the overlying mantle wedge suggests that the easiest way to explain the observed K_2O/H_2O in arc lavas is if fluid-present melting (scenario 2) at top-slab temperatures of 750–900°C occurs in the subducted sediments (Fig. 10). Although this study clarifies the nature and composition of the fluid phase present in subducted sediments, clearly more experiments are needed to constrain the interaction of these fluids with the mantle wedge for a complete understanding of LILE recycling in subduction zones.

CONCLUSIONS

(1) Phengite is the most important host for K (and other LILE) in the subducted crust. This study shows that phengite is stable to high temperatures at sub-arc depths (950°C at 3·5 GPa; 1000°C at 4·5 GPa) and hence fluid-absent phengite breakdown is not a viable process to release K from the subducted slab in most subduction zones.

(2) The pelite solidus is steeply sloping and is located at 700°C at 2·5 GPa and between 700 and 750°C at 3·5 GPa. At higher pressures we could only determine the transition from hydrous glass to non-quenchable fluid, at 800°C, 4·5 GPa. Hence, the solute content of the fluid phase released from subducted sediments will strongly increase in the temperature interval from 700 to 800°C at sub-arc depths.

(3) The K_2O and H_2O content of the fluid phase is buffered by the phengite-bearing residue and changes drastically as a function of the nature of the fluid phase and the slab temperature. Aqueous fluids, which are stable at temperatures lower than the wet solidus, are dilute and contain K_2O <1 wt% and H_2O >80 wt%. In contrast, hydrous melts display increasing K_2O and decreasing H_2O contents, with typical K_2O/H_2O of 0·1–1. Thus, efficient extraction of LILE from the subducted sediments requires wet melting.

(4) The comparison of K_2O/H_2O produced in hydrous experiments with primitive arc basalts provides evidence that the most important process for element recycling from the slab to the mantle wedge occurs via fluid-present melting of the sediments and suggests that top-slab temperatures must be in the range of 700–900°C. Once the interaction of the fluids with the mantle wedge is understood, the K_2O/H_2O of primitive arc basalts can be used to obtain independent constraints on top-slab temperatures.

ACKNOWLEDGEMENTS

We would like to thank D. Scott and W. O. Hibberson for assistance with the experiments, A. Norris and F. Brink for their help with the electron microprobe and SEM analyses, respectively, and C. Allen and M. Shelly for their help

with the ICP-MS analyses. David Green encouraged this work and provided helpful comments. We thank M. Wilson for editorial handling, and S. Poli and an anonymous reviewer for constructive comments, which helped to improve the paper. This work has been financially supported by the Australian Research Council.

SUPPLEMENTARY DATA

Supplementary data for this paper are available at *Journal of Petrology* online.

REFERENCES

Auzanneau, E., Vielzeuf, D. & Schmidt, M. W. (2006). Experimental evidence of decompression melting during exhumation of subducted continental crust. *Contributions to Mineralogy and Petrology* **152**, 125–148.

Barker, F. (1979). Trondhjemite: definition, environment and hypothesis of origin. In: Barker, F. (ed.) *Trondhjemites, Dacites and Related Rocks, Developments in Petrology*. Amsterdam: Elsevier, pp. 1–12.

Bishop, F. C., Smith, J. V. & Dawson, J. B. (1978). Na, K, P and Ti in garnet, pyroxene and olivine from peridotite and eclogite xenoliths from African kimberlites. *Lithos* **11**, 155–173.

Brunet, F., Bonneau, V. & Irifune, T. (2006). Complete solid-solution between $Na_3Al_2(PO_4)_3$ and $Mg_3Al_2(SiO_4)_3$ garnets at high pressure. *American Mineralogist* **91**, 211–215.

Carswell, D. A., O'Brien, P. J., Wilson, R. N. & Zhai, M. (1997). Thermobarometry of phengite-bearing eclogites in the Dabie Mountains of central China. *Journal of Metamorphic Geology* **15**, 239–252.

Chopin, C. (1984). Coesite and pure pyrope in highgrade blueschists of the western Alps: A first record and some consequences. *Contributions to Mineralogy and Petrology* **86**, 107–118.

Class, C., Miller, D. M., Goldstein, S. L. & Langmuir, C. H. (2000). Distinguishing melt and fluid subduction and components in Umnak volcanics, Aleutian Arc. *Geochemistry, Geophysics, Geosystems* **1**, paper number 1999GC000010.

Dickinson, W. R. (1975). Potash–depth (K–*H*) relations in continental margin and intra-oceanic magmatic arcs. *Geology* **3**, 53–56.

Domanik, K. J. & Holloway, J. R. (1996). The stability of phengitic muscovite and associated phases from 5·5 to 11 GPa: implications for deeply subducted sediments. *Geochimica et Cosmochimica Acta* **60**, 4133–4150.

Eggins, S. M., Rudnick, R. L. & McDonough, W. F. (1998). The composition of peridotites and their minerals: a laser ablation ICP-MS study. *Earth and Planetary Science Letters* **154**, 53–71.

Elliott, T. (2003). Tracers of the slab. In: Eiler, J. (ed.) *Inside the Subduction Factory*. Geophysical Monograph: American Geophysical Union **183**, 23–45.

Ellis, D. (1986). Garnet–liquid Fe^{2+}–Mg equilibria and implications for the beginning of melting in the crust and subduction zones. *American Journal of Science* **286**, 765–791.

Ellis, D. J. & Green, D. H. (1979). An experimental study of the effect of Ca upon garnet–clinopyroxene Fe–Mg exchange equilibria. *Contributions to Mineralogy and Petrology* **71**, 13–22.

Fumagalli, P. & Poli, S. (2005). Experimentally determined phase relations in hydrous peridotites to 6·5 GPa and their consequences on the dynamics of subduction zones. *Journal of Petrology* **46**, 555–578.

Green, T. H. (1977). Garnet in silicic liquids and its possible use as a *P–T* indicator. *Contributions to Mineralogy and Petrology* **65**, 59–67.

Green, T.H. & Adam, J. (2003) Experimentally-determined trace element characteristics of aqueous fluid from partially dehydrated mafic oceanic crust at 3.0 GPa, 650-700°C. *European Journal of Mineralogy* **15**, 815–830.

Green, T. H. & Hellman, P. L. (1982). Fe–Mg partitioning between coexisting garnet and phengite at high pressure, and comments on a garnet–phengite geothermometer. *Lithos* **15**, 253–266.

Hack, A. C., Hermann, J. & Mavrogenes, J. A. (2007). Mineral solubility and hydrous melting relations in the deep Earth: analysis of some binary A–H_2O system pressure–temperature–composition topologies. *American Journal of Science* **307**, 833–855.

Hawkesworth, C. J., Gallagher, K., Herget, J. M. & McDermott, F. (1993). Mantle and slab contributions in arc magmas. *Annual Review of Earth and Planetary Sciences* **21**, 175–204.

Hermann, J. (2002a). Allanite: thorium and light rare earth element carrier in subducted crust. *Chemical Geology* **192**, 289–306.

Hermann, J. (2002b). Experimental constraints on phase relations in subducted continental crust. *Contributions to Mineralogy and Petrology* **143**, 219–235.

Hermann, J. (2003). Experimental evidence for diamond-facies metamorphism in the Dora–Maira massif. *Lithos* **70**, 163–182.

Hermann, J. & Green, D. H. (2001). Experimental constraints on high pressure melting in subducted crust. *Earth and Planetary Science Letters* **188**, 149–186.

Hermann, J., Rubatto, D., Korsakov, A. & Shatsky, V. S. (2001). Multiple zircon growth during fast exhumation of diamondiferous, deeply subducted continental crust (Kokchetav massif, Kazakhstan). *Contributions to Mineralogy and Petrology* **141**, 66–82.

Hermann, J., Spandler, C., Hack, A. & Korsakov, A. V. (2006). Aqueous fluids and hydrous melts in high-pressure and ultra-high pressure rocks: Implications for element transfer in subduction zones. *Lithos* **92**, 399–417.

Huang, W. L. & Wyllie, P. J. (1981). Phase relationships of S-type granite with H_2O to 35 kbar: Muscovite granite from Harney Peak, South Dakota. *Journal of Geophysical Research* **86**, 10515–10529.

Johnson, M. C. & Plank, T. (1999). Dehydration and melting experiments constrain the fate of subducted sediments. *Geochemistry, Geophysics, Geosystems* **1**, paper number 1999GC000014.

Kelemen, P. B. & Hanghoj, K. (2003). One view of the geochemistry of subduction-related magmatic arcs, with emphasis on primitive andesite and lower crust. In: Rudnick, R. L. (ed.) *The Crust. Treatise on Geochemistry*. Amsterdam: Elsevier, pp. 593–659.

Kessel, R., Schmidt, M. W., Ulmer, P. & Pettke, T. (2005*a*). Trace element signature of subduction-zone fluids, melts and supercritical liquids at 120–180 km depth. *Nature* **437**, 724–727.

Kessel, R., Ulmer, P., Pettke, T., Schmidt, M. W. & Thompson, A. B. (2005*b*). The water–basalt system at 4 to 6 GPa: Phase relations and second critical endpoint in a K-free eclogite at 700 to 1400°C. *Earth and Planetary Science Letters* **237**, 873–892.

Kincaid, C. & Griffiths, R. W. (2004). Variability in flow and temperature within mantle subduction zones. *Geochemistry, Geophysics, Geosystems* **5**, paper number Q06002.

Konzett, J., Frost, D. J., Proyer, A. & Ulmer, P. (2007). The Ca-Eskola component in eclogitic clinopyroxene as a function of pressure, temperature and bulk composition: an experimental study to 15 GPa with possible implications for the formation of oriented SiO_2-inclusions in omphacite. *Contributions to Mineralogy and Petrology*, (in press), doi: 10.1007/s00410-007-0238-0.

Krogh Ravna, E. J. & Terry, M. P. (2004). Geothermobarometry of UHP and HP eclogites and schists—an evaluation of equilibria

among garnet–clinopyroxene–kyanite–phengite–coesite/quartz. *Journal of Metamorphic Geology* **22**, 579–592.

Lang, H. M. & Gilotti, J. A. (2007). Partial melting of metapelites at ultrahigh-pressure condition, Greenland Caledonides. *Journal of Metamorphic Geology* **25**, 129–147.

Liu, J., Bohlen, S. R. & Ernst, W. G. (1996). Stability of hydrous phases in subducting oceanic crust. *Earth and Planetary Science Letters* **143**, 161–171.

Malaspina, N., Hermann, J., Scambelluri, M. & Compagnoni, R. (2005). Multistage metasomatism in ultrahigh-pressure mafic rocks from the North Dabie Complex (China). *Lithos* **90**, 19–42.

Malaspina, N., Hermann, J., Scambelluri, M. & Compagnoni, R. (2006). Polyphase inclusions in garnet-orthopyroxenite (Dabie Shan, China) as monitors for metasomatism and fluid related trace element transfer in subduction zone peridotite. *Earth and Planetary Science Letters* **249**, 173–187.

Manning, C. E. (1998). Fluid composition at the blueschist–eclogite transition in the model system Na_2O–MgO–Al_2O_3–SiO_2–H_2O–HCl. *Schweizerische Mineralogische und Petrographische Mitteilungen* **78**, 225–242.

Manning, C. E. (2004). The chemistry of subduction-zone fluids. *Earth and Planetary Science Letters* **223**, 1–16.

Massonne, H.-J. (2003). A comparison of the evolution of diamondiferous quartz-rich rocks from the Saxonian Erzgebirge and the Kokchetav Massif: are so-called diamondiferous gneisses magmatic rocks? *Earth and Planetary Science Letters* **216**, 347–364.

Massonne, H.-J. & Nasdala, L. (2003). Characterization of an early metamorphic stage through inclusions in zircon of a diamondiferous quartzofeldspathic rock from the Erzgebirge, Germany. *American Mineralogist* **88**, 883–889.

Massonne, H.-J. & Schreyer, W. (1987). Phengite geobarometry based on the limiting assemblage with K-feldspar, phlogopite and quartz. *Contributions to Mineralogy and Petrology* **96**, 212–224.

Massonne, H.-J. & Szpurzka, Z. (1997). Thermodynamic properties of white micas on the basis of high-pressure experiments in the systems K_2O–MgO–Al_2O_3–SiO_2–H_2O and K_2O–FeO–Al_2O_3–SiO_2–H_2O. *Lithos* **41**, 229–250.

Meyre, C., De Capitani, C., Zack, T. & Frey, M. (1999). Petrology of high-pressure metapelites from the Adula Nappe (Central Alps, Switzerland). *Journal of Petrology* **40**, 199–213.

Mposkos, E. D. & Kostopoulos, D. K. (2001). Diamond, former coesite and supersilic garnet in metasedimentary rocks from the Greek Rhodope: a new ultrahigh-pressure metamorphic province established. *Earth and Planetary Science Letters* **192**, 497–506.

Nichols, G. T., Wyllie, P. J. & Stern, C. R. (1994). Subduction zone melting of pelagic sediments constrained by melting experiments. *Nature* **371**, 785–788.

Ono, S. (1998). Stability limits of hydrous minerals in sediment and mid-ocean ridge basalt compositions: implications for water transport in subduction zones. *Journal of Geophysical Research* **103**, 18253–18267.

Patiño Douce, A. E. (2005). Vapor-absent melting of tonalite at 15–32 kbar. *Journal of Petrology* **46**, 275–290.

Patiño Douce, A. E. & McCarthy, T. C. (1998). Melting of crustal rocks during continental collision and subduction. In: Hacker, B. R. & Liou, J. G. (eds) *When Continents Collide: Geodynamics and Geochemistry of Ultrahigh-Pressure Rocks*. Dordrecht: Kluwer Academic, pp. 27–55.

Peacock, S. M., Rushmer, T. & Thompson, A. B. (1994). Partial melting of subducted oceanic crust. *Earth and Planetary Science Letters* **121**, 227–244.

Pearce, N. J. G., Perkins, W. T., Westgate, J. A., Gorton, M. P., Jackson, S. E., Neal, C. R. & Chenery, S. P. (1997). A compilation of new and published major and trace element data for NIST SRM 610 and NIST SRM 612 glass reference materials. *Geostandards News* **21**, 115–144.

Peate, D. W., Pearce, J. A., Hawkesworth, C. J., Colley, H., Edwards, C. M. H. & Hirose, K. (1997). Geochemical variations in Vanuatu arc lavas: the role of subducted material and a variable mantle wedge composition. *Journal of Petrology* **38**, 1331–1358.

Philippot, P., Chevallier, P., Chopin, C. & Debussy, J. (1995). Fluid composition and evolution in coesite-bearing rocks (Dora–Maira massif, Western Alps): Implications for element recycling during subduction. *Contributions to Mineralogy and Petrology* **121**, 29–44.

Plank, T. & Langmuir, C. H. (1993). Tracing trace elements from sediment input to volcanic output at subduction zones. *Nature* **362**, 739–743.

Plank, T. & Langmuir, C. H. (1998). The chemical composition of subducting sediments and its consequences for the crust and mantle. *Chemical Geology* **145**, 325–394.

Poli, S. & Schmidt, M. W. (2002). Petrology of subducted slabs. *Annual Review of Earth and Planetary Sciences* **30**, 207–235.

Portnyagin, M., Hoernle, K., Plechov, P., Mironov, N. & Khubunaya, S. (2007). Constraints on mantle melting and composition and nature of slab components in volcanic arcs from volatiles (H_2O, S, Cl, F) and trace elements in melt inclusions from the Kamchatka Arc. *Earth and Planetary Science Letters* **255**, 53–69.

Powell, R. & Holland, T. (1990). Calculated mineral equilibria in the pelite system, KFMASH (K_2O–FeO–MgO–Al_2O_3–SiO_2–H_2O). *American Mineralogist* **75**, 367–380.

Ringwood, A. E. & Major, A. (1971). Synthesis of majorite and other high-pressure garnets and perovskites. *Earth and Planetary Science Letters* **12**, 411–441.

Rubatto, D. & Hermann, J. (2007). Experimental zircon/melt and zircon/garnet trace element partitioning and implications for the geochronology of crustal rocks. *Chemical Geology* **241**, 38–61.

Salters, V. J. M. & Stracke, A. (2004). Composition of the depleted mantle. *Geochemistry, Geophysics, Geosystems* **5**, paper number Q05004.

Schmädicke, E. & Müller, W. F. (2000). Unusual exsolution phenomena in omphacite and partial replacement of phengite by phlogopite + kyanite in an eclogite from the Erzgebirge. *Contributions to Mineralogy and Petrology* **139**, 629–642.

Schmidt, M. W. (1996). Experimental constraints on recycling of potassium from subducted oceanic crust. *Science* **272**, 1927–1930.

Schmidt, M. W., Vielzeuf, D. & Auzanneau, E. (2004). Melting and dissolution of subducting crust at high pressures: the key role of white mica. *Earth and Planetary Science Letters* **228**, 65–84.

Sekine, T. & Wyllie, P. J. (1982). Phase relationships in the system $KAlSiO_4$–Mg_2SiO_4–SiO_2–H_2O as a model for hybridization between hydrous siliceous melts and peridotite. *Contributions to Mineralogy and Petrology* **79**, 368–374.

Sobolev, A. V. & Chaussidon, M. (1996). H_2O concentrations in primary melts from supra-subduction zones and mid-ocean ridges: Implications for H_2O storage and recycling in the mantle. *Earth and Planetary Science Letters* **137**, 45–55.

Sobolev, N. V. & Lavrent'ev, J. G. (1971). Isomorphic sodium admixture in garnets formed at high pressures. *Contributions to Mineralogy and Petrology* **31**, 1–12.

Sobolev, N. V. & Shatsky, V. S. (1990). Diamond inclusions in garnets from metamorphic rocks: A new environment for diamond formation. *Nature* **343**, 742–746.

Sorenson, S. S., Grossman, J. N. & Perfit, M. R. (1997). Phengite-hosted LILE enrichment in eclogite and related rocks: implications for fluid-mediated mass transfer in subduction zones and arc magma genesis. *Journal of Petrology* **38**, 3–34.

Spandler, C. J., Hermann, J., Arculus, R. J. & Mavrogenes, J. A. (2003). Redistribution of trace elements during prograde metamorphism from lawsonite blueschist to eclogite facies; implications for deep subduction-zone processes. *Contributions to Mineralogy and Petrology* **146**, 205–222.

Spandler, C., Hermann, J., Faure, K., Mavrogenes, J. A. & Arculus, R. J. (2007*a*). The importance of talc and chlorite 'hybrid' rocks for volatile recycling through subduction zones; evidence from the high-pressure subduction mélange of New Caledonia. *Contributions to Mineralogy and Petrology* (in press), doi: 10.1007/s00410-007-0236-2.

Spandler, C., Mavrogenes, J. A. & Hermann, J. (2007*b*). Experimental constraints on element mobility from subducted sediments using high-*P* synthetic fluid/melt inclusions. *Chemical Geology* **239**, 228–249.

Stern, R. J. (2002). Subduction zones. *Reviews of Geophysics* **40**, doi: 2001RG000108.

Stöckhert, B., Duyster, J., Trepman, C. & Massone, H.-J. (2001). Microdiamond daughter crystals precipitated from supercritical COH + silicate fluids included in garnet, Erzgebirge, Germany. *Geology* **29**, 391–394.

Syracuse, E. M. & Abers, G. A. (2006). Global compilation of variations in slab depth beneath arc volcanoes and implications. *Geochemistry, Geophysics, Geosystems* **7**, paper number Q05017.

Tatsumi, Y. (1986). Formation of the volcanic front in subduction zones. *Geophysical Research Letters* **17**, 717–720.

Tatsumi, Y. & Eggins, S. M. (1995). *Subduction Zone Magmatism*. Cambridge: Blackwell.

Taylor, S. R. & McLennan, S. M. (1985). *The Continental Crust: its Composition and Evolution*. Oxford: Blackwell.

Tenthorey, E. & Hermann, J. (2004). Composition of fluids during serpentinite breakdown in subduction zones: Evidence for limited boron mobility. *Geology* **32**, 865–868.

Thompson, R. N. (1975). Is upper mantle phosphorus contained in sodic garnet? *Earth and Planetary Science Letters* **26**, 417–424.

van Keken, P. E., Kiefer, B. & Peacock, S. M. (2002). High-resolution models of subduction zones: Implications for mineral dehydration reactions and the transport of water into the deep mantle. *Geochemistry, Geophysics, Geosystems* **3**, doi:10.1029/2001GC000256.

Vielzeuf, D. & Holloway, J. R. (1988). Experimental determination of the fluid-absent melting relations in the pelitic system. *Contributions to Mineralogy and Petrology* **98**, 257–276.

Yardley, B. W. D. (1989). *An Introduction to Metamorphic Petrology*. Harlow: Longman.

Ye, K., Cong, B. & Ye, D. (2000). The possible subduction of continental material to depths greater than 200 km. *Nature* **407**, 734–736.

Zhang, R. Y., Liou, J. G., Ernst, W. G., Coleman, R. G., Sobolev, N. V. & Shatsky, V. S. (1997). Metamorphic evolution of diamond-bearing and associated rocks from the Kokchetav Massif, Northern Kazakhstan. *Journal of Metamorphic Geology* **15**, 479–496.